ANTHROPOLOGY

Pilgrimage to sacrifice: Mechanisms, causes, and time of death of the Western Andean Capacocha of the Southern Tawantinsuyu

Verónica Silva-Pinto[1,2,3]*†, Marcela Sepúlveda[4]†, Eugenia M. Gayo[5,6,7]†, Pablo Mendez-Quiros[8], Mario Castro[9,10], Lumila Paula Menéndez[11,12], Gonzalo M. Rojas-Costa[13,14], María L. Cerón[15], Andrew S. Wilson[16], Verónica Catalán[17,18], Claudio Silva[19], Ximena Stecher[19], Pablo Soffia[19], Domingo C. Salazar-García[20,21]*

Capacocha was a key Inca state rite that intertwined pilgrimage, sacrifice, and imperial incorporation across the Andes. We present a multianalytical investigation into two Capacocha cases from the western slope of the Andes: Cerro Esmeralda, located in the coastal Atacama Desert of northern Chile, and Cerro El Plomo, in the high mountains of central Chile. Stable isotope analysis reveals commensality practices during the pilgrimage, integrating local communities into the imperial order. Furthermore, computed tomography, dermatoscopy, and skin histology provide new evidence regarding the causes and mechanisms of death, identifying violent acts associated with sacrifice. Last, we present a pair of radiocarbon dates to discuss the chronology of both Capacocha contexts. In sum, these practices specify the materialization of Inca statecraft and contribute to characterizing the complexity and diversity of Capacocha ritual as an extension of the Inca biopolitical conquest.

INTRODUCTION

Human sacrifice is a powerful ritual practice and an act of devotion embedded within religious systems, used not only for spiritual purposes but also as a means of economic appropriation, ideological reinforcement, consolidation of authority, and coercive control over subjected populations within expanding states (*1*–*5*). Among the Incas, the Capacocha (Qhapaq Hucha) was one of the most notable sacrificial rituals. In this ceremonial practice, human bodies were offered to the mountains, or apus, which were considered sacred places, powerful ancestors, and Huacas (sacred beings) (*6*, *7*). The sacrificed children were not merely offerings but were believed to enter the sacred world of the apus, becoming divine beings and intermediaries between their communities and the gods (*8*, *9*). This transformation framed death as a change in status: After sacrifice, the children became Huacas themselves, mediators of energy and meaning within the sacred landscape (*10*, *11*). Capacocha ritual thus constituted a complex network of human and nonhuman entities (*12*–*14*), a remarkable ceremonial practice through which an entangled sacred geography was established (*15*, *16*). As persistent places, these ritual landscapes constitute assemblages of human and nonhuman phenomena (*17*). They reinforced a process that can be understood as a form of biopolitical conquest within Tawantinsuyu, in which the human body, through sacrifice, implied the offering of its vitality to the apus (*18*). As noted, "the integration of human and nonhuman persons into a ritualized community of food sharing energy transfer can be understood as intrinsically biopolitical" (*18*). In this scenario, "wak'as and landscape were symbolically, socially, and even physiologically entangled and interdependent" (*19*). Studying the Capacocha ritual can therefore illuminate the complexity of the Inca imperial expansion.

In the Capacocha ritual, pilgrimage was a central component of the ceremonial structure. Pilgrimage connected sacred landscapes and administrative centers through ritual journeys and processions that inscribed political and religious authority across space (*20*–*25*). This rite carried exceptional symbolic and political importance, linking distant regions to the imperial core through embodied acts of devotion and allegiance. As both a political and religious process (*26*, *27*), the pilgrimage involved not only the actions of the entourage and those making the offering but also the active participation of local communities through commensal ceremonies (*28*, *29*). These interactions helped captivate and spiritually integrate conquered populations, reinforcing their symbolic subordination and their contribution to the physical and ideological unification of the empire and its diverse inhabitants (*30*).

Selected for their perceived purity and exceptional beauty, the individuals chosen for sacrifice were either taken from their home communities or offered by local authorities (*10*, *13*, *31*). They were brought to Cuzco, the political and ceremonial heart of the empire,

[1]Programa de Doctorado en Geografía e Historia del Mediterráneo desde la Prehistoria a la Edad Moderna, Universitat de València, València, Spain. [2]Escuela de Antropología, Facultad de Ciencias Sociales e Historia, Universidad Diego Portales, Santiago, Chile. [3]Área de Antropología, Museo Nacional de Historia Natural, Santiago, Chile. [4]Departamento de Ciencias Sociales, Universidad de Tarapacá, Iquique, Chile. [5]Departamento de Geografía, Universidad de Chile, Santiago, Chile. [6]Center for Climate and Resilience Research (CR2), Santiago, Chile. [7]Institute of Ecology and Biodiversity (IEB), Concepción, Chile. [8]Departamento de Antropología, Universidad de Chile, Santiago, Chile. [9]Museo Nacional de Historia Natural, Santiago, Chile. [10]Departamento de Morfología, Facultad de Medicina, Clínica Alemana–Universidad del Desarrollo, Santiago, Chile. [11]Department of Anthropology of the Americas, University of Bonn, Bonn, Germany. [12]Department of Evolutionary Biology, University of Vienna, Vienna, Austria. [13]School of Medicine, Finis Terrae University, 7501015 Santiago, Chile. [14]Biomedical Imaging Unit and Artificial Intelligence FISABIO-CIPF, Foundation for the Promotion of Health and Biomedical Research of the Valencia Region, València, Spain. [15]Facultad de Ingeniería, Universidad Finis Terrae, Santiago, Chile. [16]School of Archaeological and Forensic Sciences, University of Bradford, Bradford, UK. [17]Servicio de Dermatología, Clínica Alemana–Universidad del Desarrollo, Santiago, Chile. [18]Departamento de Dermatología, Facultad de Medicina, Universidad de Chile, Santiago, Chile. [19]Departamento de Imagenología, Facultad de Medicina, Clínica Alemana-Universidad del Desarrollo, Santiago, Chile. [20]Departament de Prehistòria, Arqueologia i Història Antiga, Universitat de València, València, Spain. [21]Department of Geological Sciences, University of Cape Town, Cape Town, South Africa.
*Corresponding author. Email: veronica.silva1@mail.udp.cl (V.S.-P.); domingocarlos.salazar@uv.es (D.C.S.-G.)
†These authors contributed equally to this work.

from where they embarked on pilgrimage to remote shrines (*32*–*34*). From there, they undertook a long, final journey to sacred mountain summits, where they were ritually killed (*2*, *10*, *35*, *36*). The final ascent to the summit followed specific routes, transforming the experience of movement into one of spiritual transition through an Inca-defined landscape (*21*, *37*, *38*). As Kantner and Vaughn (*39*) suggest, these pilgrimage practices also functioned as "costly signals": highly visible and resource-intensive performances of piety and loyalty that reinforced imperial power and fostered cooperation across diverse provincial groups.

Therefore, understanding the Capacocha is essential for understanding the mechanisms of Inca imperial expansion into the southern Andes and the conquest of much of South America. A major challenge lies in accurately reconstructing the pilgrimage process of the Capacocha ritual—including the circumstances and methods of sacrifice, as well as the timing and context of these acts—while adhering to ethical standards.

This study examines two Capacocha contexts from Chile (Fig. 1). The first involves two females from Cerro Esmeralda, a site located at 905 m above sea level (masl) in the Atacama Desert of northern Chile: a 9-year-old female individual, Cerro Esmeralda-A (CES-A) and an 18-year-old female individual, Cerro Esmeralda-B (CES-B). Discovered in 1976 after the tomb was partially destroyed with dynamite, their naturally mummified bodies exhibit substantial alterations resulting from uncontrolled recovery and subsequent autopsies. Both individuals are curated at the Regional Museum of Iquique.

The second case concerns an 8-year-old male individual, Niño de El Plomo (NEP) from Cerro El Plomo, discovered in 1954 at 5400 masl

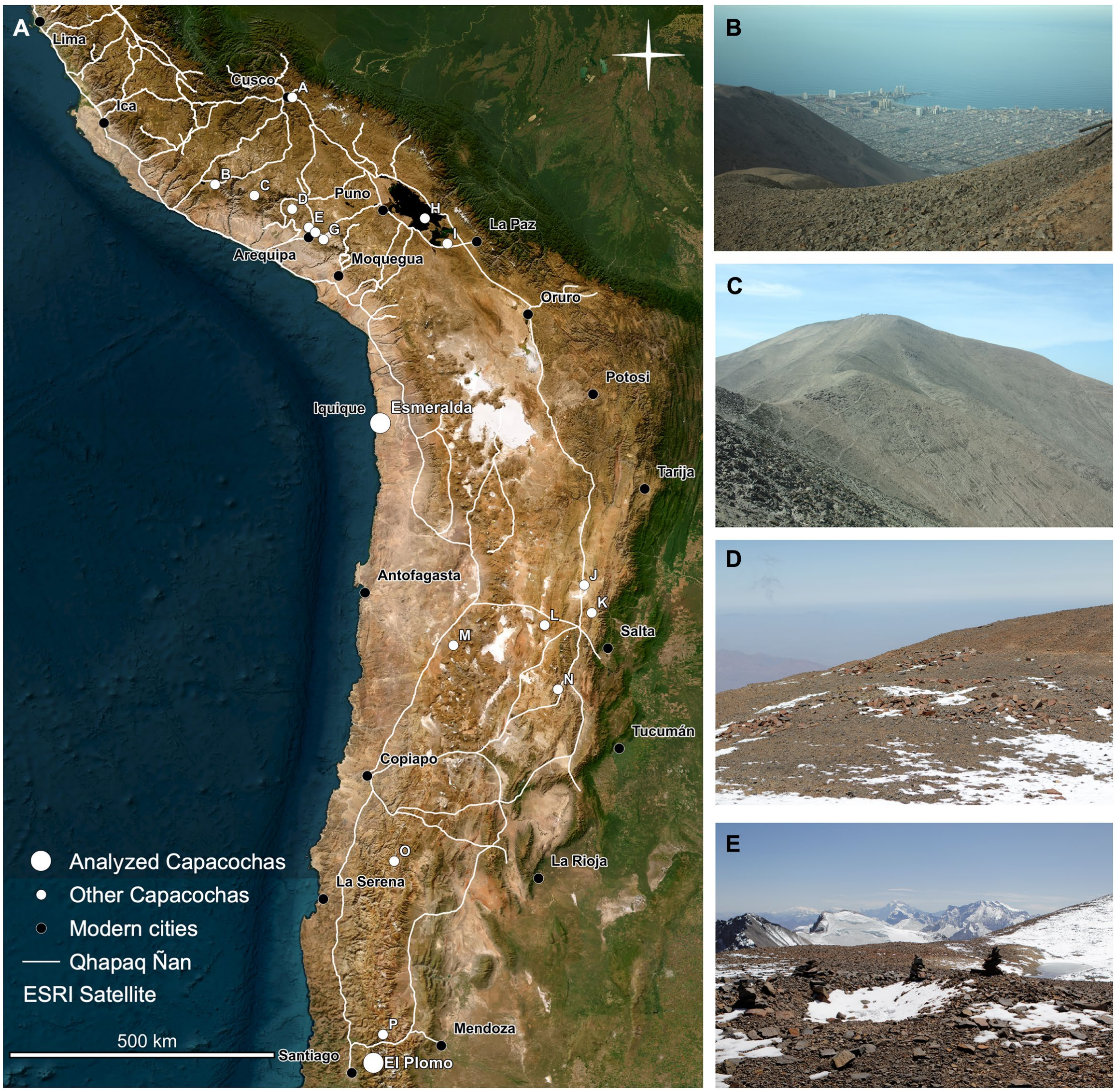

Fig. 1. Location of documented Capacocha sites in the Central and South-Central Andes. (**A**) Map showing the distribution of Capacocha sites and their relationship to the Qhapaq Ñan network: A, Choquepukio; B, Sara Sara; C, Coropuna; D, Ampato; E, Chachani; F, Misti; G, Pichu Pichu; H, Isla del Sol; I, Tiwanaku; J, Salinas Grandes; K, Chañi; L, Quehuar; M, Llullaillaco; N, Chuscha; O, El Toro; P, Aconcagua [Proyecto Qhapaq Ñan Sede Nacional (Perú); adapted from Hyslop, 1984). (**B**) View of the city of Iquique from Cerro Esmeralda. (**C**) Overview of Cerro Esmeralda (950 masl). (**D**) Burial site of the El Plomo child (5400 masl). (**E**) Burial pit surrounded by stones. Photo credits: (B and C) Photographs by P. Mendez-Quiroz; (D and E) photographs by J. Gamboa, used with permission. ESRI, Environmental Systems Research Institute.

in the high Andes of central Chile by treasure hunters. The body was naturally preserved under freezing conditions and has been curated since 1954 at the National Museum of Natural History in Santiago, where it is housed in a cold chamber ($T = -4° \pm 2°C$; relative humidity, RH = 68 ± 5%). In both cases, the original recoveries lacked archaeological control, limiting the contextual information available.

To reconstruct the life histories, dietary patterns, mobility trajectories, and perimortem circumstances of these individuals, as well as the broader ceremonial framework, we conducted multi-isotopic analyses ($\delta^{13}C$, $\delta^{15}N$, $\delta^{34}S$, $\delta^{18}O$, and $\delta^{2}H$ on hair), dermatoscopic examinations, high-resolution computed tomography (CT) scanning, and radiocarbon dating. We further evaluated the hypothesis that these individuals participated in ritualized commensality during pilgrimage, reflecting their integration into the Inca imperial system through food provisioning and symbolic exchange. To investigate this, we applied regime shift analysis to the isotopic data to identify periods of marked structural change in each individual's life history (table S2).

These datasets enable a more refined interpretation of sacrificial contexts and provide a framework for testing specific hypotheses regarding the causes of death and ritual function. In particular, we revisit prior interpretations of strangulation in CES-A and CES-B, and hypothermia in NEP, integrating new forensic and bioarchaeological evidence.

For the Cerro Esmeralda individuals, we reassessed Checura's (*40*) original proposal, which identified linear impressions on the neck interpreted as possible ligature marks—potential indicators of strangulation. This form of mechanical asphyxia is notoriously difficult to confirm in nonadults due to minimal external trauma and the incomplete ossification of the hyoid bone (*41–43*). Strangulation may result from vascular compression (20 to 100 N), airway obstruction (8 to 12 kg), or vagus nerve–mediated neurogenic reflexes (*44–46*). Although hyoid fractures are considered diagnostic of strangulation, they occur in fewer than half of adult cases and are even rarer in children and adolescents due to the bone's elasticity (*47*, *48*).

In the case of NEP, Mostny's (*49*) hypothesis of hypothermic death was originally based on the presumed cold-induced necrosis of several fingers, along with the apparent absence of traumatic injury. The exceptional preservation of the body enabled the application of dermatoscopic, histological, and tomographic analyses. In addition, we generated three-dimensional (3D) reconstructions of the cranium and applied finite element analysis (FEA), representing the first archaeological application of this method in a Capacocha context to our knowledge. While FEA has proven effective in forensic investigations of blunt force and ballistic cranial trauma (*50–53*), its potential for paleopathological research remains largely unexplored.

Last, we obtained five new paired radiocarbon dates from hair, bone, and textile samples to refine the chronology of the Capacocha rituals at Cerro Esmeralda and Cerro El Plomo. These results were compared with published dates from similar ritual contexts and with the timeline of Inca expansion in the Collasuyu, enabling us to situate these sacrifices within the broader imperial conquest of the southern Andes. To address these questions, our study used nondestructive and minimally invasive techniques, using limited sampling to preserve the integrity of the human remains and associated offerings.

RESULTS

Shifts in stable isotope signatures in sequential hair

The $\delta^{13}C$ and $\delta^{15}N$ values of CES-A exhibit covariation throughout the sequential analysis of hair samples (Fig. 2 and table S1). Before the steady increase observed toward death (0.5 cm from the scalp), both $\delta^{13}C$ and $\delta^{15}N$ values remain low between 11.5 and 5.5 cm. Over this interval, $\delta^{13}C$ values rise from −16.99 to −13.44 per mil (‰), while $\delta^{15}N$ increases from 9.02 to 14.27‰. These shifts are marked by statistically significant regime changes: $\delta^{13}C$ at 5.5 cm [regime shift index (RSI) = 0.68] and the carbon-nitrogen change index (C-N index) at 7.5 cm (RSI = 1.36) (table S2). Despite this overall trend, $\delta^{15}N$ values remain relatively stable between 11.5 and 5.5 cm (+9.11 to +10.06‰), in contrast to the more pronounced variation observed in $\delta^{13}C$ across the same segment (−15.76 to −16.03‰) (Fig. 2 and table S1). $\delta^{34}S$ values remain stable (+11.55 to +11.28‰) from ~14 to 9 months before death (14 to 9 cm) (Fig. 2 and table S1). A statistically significant regime shift at 9 cm (RSI = 1.46) marks the onset of a consistent decline in $\delta^{34}S$ values (table S2), decreasing from +11.55‰ at 14 months before death to +9.53‰ in the month preceding death (Fig. 2 and table S1).

In the CES-B individual, $\delta^{13}C$ values show limited variation between 17 and 3 cm, fluctuating within a narrow range from +10.12 to +11.94‰. Similarly, $\delta^{15}N$ values remain relatively stable between 3.5 and 16 cm, with minimal fluctuations ranging from +9.87 to +10.52‰ (Fig. 2 and table S1). However, both carbon and nitrogen isotopic signatures increase rapidly beginning in the third month before death, although these changes do not correspond to statistically significant regime shifts (table S2). $\delta^{34}S$ values show minimal variation between 17 and 13 months before death (+10.83 to +11.43‰), followed by a sharp decline at 12.5 cm (Fig. 2 and table S1). From 12 to 3 months before death, sulfur isotope values rise again, fluctuating between +11.48 and +11.98‰. A progressive decline is then observed over the final two and a half months of life, with $\delta^{34}S$ values decreasing from +10.94 to +10.48‰. This decline corresponds to a statistically significant regime shift (RSI = 1.25) (table S2). Oxygen stable isotope values show minor fluctuations throughout the hair sequence, ranging from +8.61 to +10.73‰, between 18 and 1.0 cm, with no discernible trend (Fig. 2 and table S1). In contrast, $\delta^{2}H$ values follow a more structured pattern: an initial decline from the 18th to the 12th month before death (−90.39 to −102.05‰), a brief increase from the 11th to the 9th month (−96.53 to −94.95‰), and a renewed decrease between the 8th and 5th months (−99.53 to −103.98‰). During the final 4 months of life, $\delta^{2}H$ values increase abruptly from −98.25 to −81.84‰; however, this shift is not statistically significant (table S2).

The NEP individual exhibits distinct stable isotope variations across multiple elements in the months preceding death (Fig. 2 and table S1). $\delta^{13}C$ values show a progressive increase from −15.16‰ at 18 months before death (18 cm) to −9.74‰ at ~7.5 months (7.5 cm), followed by a gradual decline to −13.05‰ in the final months (1.5 cm). Because of the gradual nature of these changes, no statistically significant regime shifts were detected in the $\delta^{13}C$ time series (table S2). In contrast, $\delta^{15}N$ values display a statistically significant regime shift at 12 months before death (RSI = 2.14), marking a transition from a higher range (+9.95 to +9.27‰ between 18 and 12 cm) to a lower range (+8.67 to +8.20‰ between 11 and 3 cm), ultimately reaching +7.58‰ in the final month (1.5 cm) (Fig. 2 and table S1). An additional regime shift was detected in the C-N index (RSI = 0.25) at 7.5 cm (table S2). $\delta^{34}S$ values remain relatively stable between +7.48 and +7.40‰ from 14 to 11 months before death, followed by a sharp increase to +8.10‰ at 9 months. This pattern is followed by a rapid decline to +7.21‰ at 8 cm and +6.92‰ at 6 cm. During the final months of life (4.5 to 1.5 cm), $\delta^{34}S$ values stabilize again,

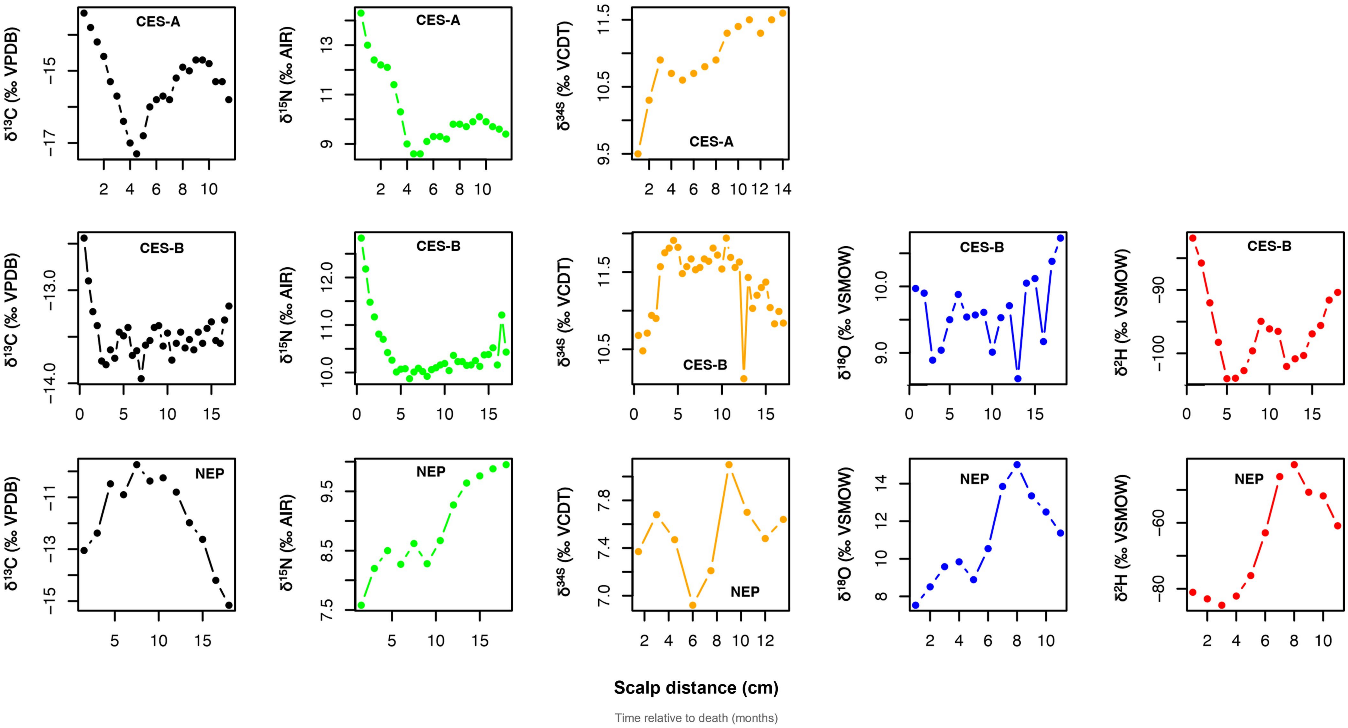

Fig. 2. Temporal changes in stable isotope composition along the hair profiles of the Cerro Esmeralda (CES-A and CES-B) and El Plomo (NEP) individuals. Distance from the scalp (in centimeters) was converted to months before death assuming a constant hair growth rate of 1 cm/month. Lower *x*-axis values correspond to periods closer to death, whereas higher values represent earlier periods. Black, green, orange, blue, and gray dotted curves indicate $\delta^{13}C$, $\delta^{15}N$, $\delta^{34}S$, $\delta^{18}O$, and $\delta^{2}H$, respectively.

fluctuating between +7.68 and +7.37‰. No statistically significant regime shifts were detected in the $\delta^{34}S$ series. Oxygen and hydrogen stable isotope signatures covary throughout the documented trajectory (i.e., the pilgrimage). Both $\delta^{18}O$ and $\delta^{2}H$ values increase gradually between 11 and 8 months before death, from +11.37 to +15.01‰ for $\delta^{18}O$ and from −60.89 to −42.33‰ for $\delta^{2}H$. This upward trend is followed by a sharp decline, with statistically significant regime shifts detected at 7.5 cm for $\delta^{18}O$ (RSI = 1.45) and 7 cm for $\delta^{2}H$ (RSI = 1.65) (table S2). A concurrent regime shift was also observed in the oxygen-hydrogen index (O-H index) at 7.5 cm (RSI = 1.97).

Reexamining causes of death and perimortem injury patterns

External examination and CT scanning of CES-A and CES-B (Fig. 3, A to F) reveal extensive anthropogenic alterations attributable to recovery handling and subsequent interventions (Fig. 3, B and E). CES-A presents a perforation in the right hypochondrium, with associated rib fractures and loss of costal cartilage, as previously reported by Checura (*40*) (Fig. 3, B to D). During the 1977 autopsy, the thoracoabdominal organs were removed through this preexisting perforation. CES-A also exhibits scalp incisions and epiphyseal cuts consistent with anthropometric examination. By contrast, CES-B shows a more systematic autopsy-related incision pattern, along with incisions comparable to those observed in CES-A and evidence of postrecovery disarticulation (Fig. 3, E and F). Notably, both individuals retain bifurcated hairstyles secured with tulmas (pompons) (Fig. 3, G and H).

CT-based assessment estimates the biological age of female CES-A at 9 to 10 years old (Fig. 3, I and J) and female CES-B at 18 to 19 years old. Despite extensive postmortem disturbance, the hyoid bones in both individuals are well preserved and remain at the expected anatomical level (approximately C3) (Fig. 3, K and L), with no fractures, displacement, or other evidence of cervical trauma. Linear superficial impressions on the neck skin are more consistent with textile or garment compression than with ligature marks. Together, these observations do not support the strangulation hypothesis proposed by Checura (*40*). No conclusive evidence of perimortem violence could be identified in either individual.

External examination and histological analysis of NEP reveal a well-preserved body with intact skin and no visible evidence of antemortem freezing or cold-induced damage to the extremities (fig. S1, A to F). Dermatoglyphs and acrosyringia are clearly preserved on the plantar surfaces, and histology shows no evidence of inflammation or tissue degeneration (fig. S1, G to I). The plantar skin exhibits dark-brown exogenous pigmentation and marked hyperkeratosis (*54*), consistent with sustained frictional loading.

CT-based assessment estimates NEP's biological age at death as 8 to 9 years (Fig. 4 and fig. S2, A to D). An oval skin lesion is present on the left frontal region (36.6 mm by 20.5 mm), characterized by a shallow depression and localized inflammatory changes (Fig. 4, A to C). Directly beneath the center of this lesion, CT imaging reveals a linear perimortem fracture of the left frontal bone near the temporal line (29.7 mm) (Fig. 4D). The spatial correspondence between the external lesion and the fracture indicates a single impact focus. The cranial trauma is further associated with traumatic diastasis of ~140 mm

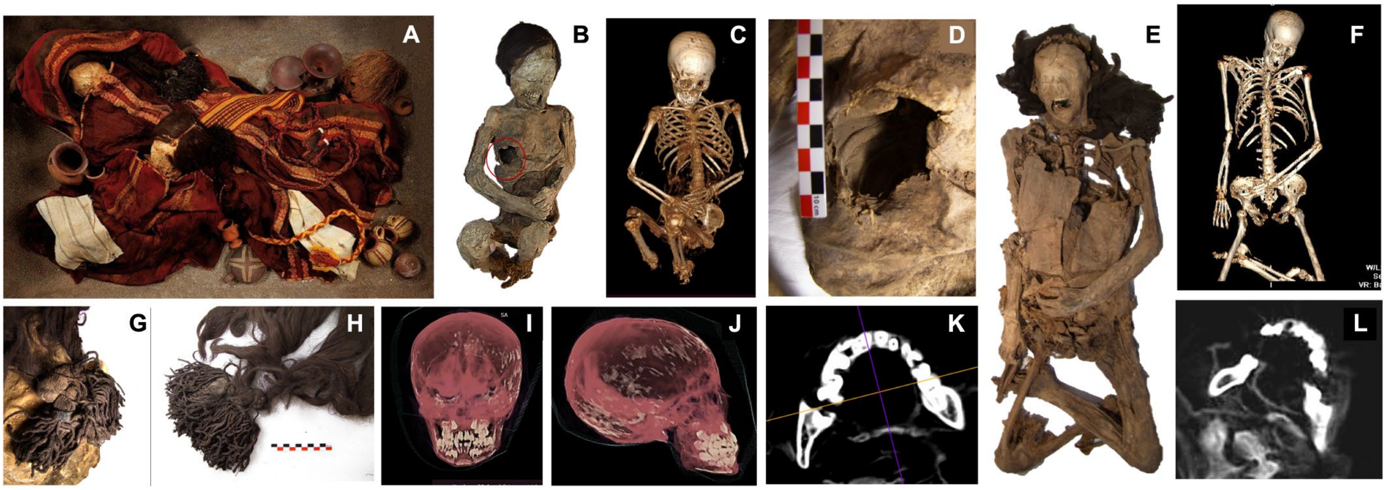

Fig. 3. Cerro Esmeralda individuals. (**A**) Museum display of CES-A and CES-B at the Museo Regional de Iquique before 2011. (**B**) Anterior view of CES-A, a female child; the red circle indicates a perforation in the right hypochondrium. (**C**) 3D reconstruction of CES-A, anterior view. (**D**) Close-up of the hypochondrial perforation in CES-A. (**E**) Anterior view of CES-B, a juvenile female. (**F**) 3D reconstruction of CES-B, anterior view. (**G**) CES-A hairstyle with tulmas; radiocarbon samples were obtained from this context. (**H**) CES-B hairstyle with tulmas; radiocarbon samples were obtained from this context. (**I** and **J**) 3D rendering of the CES-A skull with transparency showing dental development: (I) anterior view and (J) right lateral view. (**K**) CT slice of CES-A showing the hyoid bone, transverse view. (**L**) CT slice of CES-B showing the hyoid bone, transverse view. Photo credits: (A) Archivo Administrativo, Museo Regional de Iquique–CORMUDESI; [(B), (D), (E), (G), and (H)] photographs by M. Alarcón, courtesy of Archivo Administrativo, Museo Regional de Iquique–CORMUDESI.

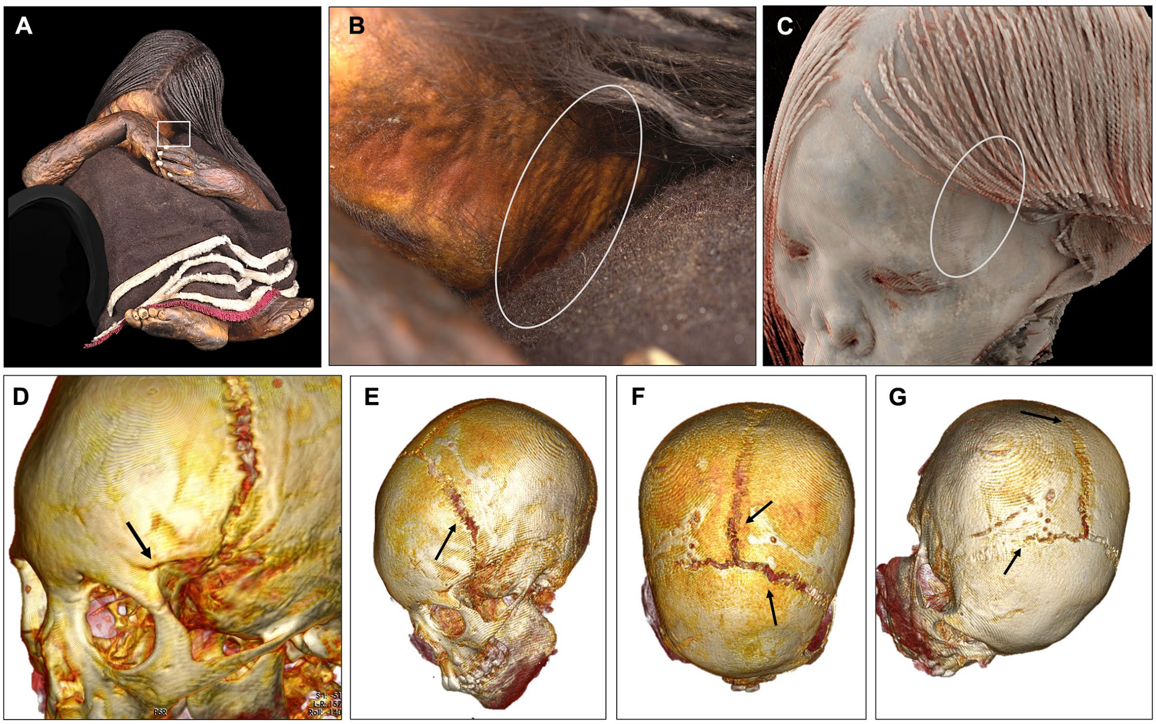

Fig. 4. Visualization of skin and cranial injury in the El Plomo child (NEP). (**A**) Anterior photograph of NEP; the injury area is marked with a white rectangle. (**B**) Close-up of the skin lesion; the indentation is marked with a white oval. (**C**) 3D CT rendering of the injury area (white oval). (**D**) 3D CT rendering showing the frontal fracture line (black arrow). (**E**) 3D CT rendering showing traumatic diastasis of the coronal suture (black arrow). (**F**) 3D CT rendering showing traumatic diastasis of the coronal and sagittal sutures (black arrows). (**G**) 3D CT rendering showing the termination point of the diastasis in the coronal and sagittal sutures (black arrows). Photo credits: [(A) and (B)] Colección Museo Nacional de Historia Natural, Chile/Archivo Centro Nacional de Conservación y Restauración (CNCR), P. Monteverde, 2023.

along the coronal suture and ~70 mm along the sagittal suture (Fig. 4, E to G). CT imaging also reveals a dilated esophagus and a stomach containing food remains (fig. S2, E and F).

The cranial injury pattern supports a closed blunt impact mechanism. A CT-derived finite element model of NEP's left hemicranium was used to define the simulation geometry and impact footprint (Fig. 5, A and D). Among the candidate implements evaluated, a blunt-lobed lithic star-shaped mace head produced the closest match to the lesion footprint and was therefore used to define the modeled contact/loading area (Fig. 5, B and C).

These findings prompted an assessment of the biomechanical plausibility of blunt force trauma as the source of the observed cranial damage. FEAs indicate that the simulated loads generate tensile stresses exceeding published failure thresholds for juvenile cranial bone (*55*, *56*) and produce deformation values consistent with the cranial thickness at the impact site. Specifically, a force of 2800 N yielded a deformation of 2.44 mm, closely matching the measured local cranial thickness (2.448 mm). The nonlinear dynamic simulation using the same force produced peak stresses of ~180 MPa and a deformation of 2.95 mm (Fig. 5, E and F, and Table 1). Together, these results support the biomechanical plausibility that a high-energy blunt impact could account for the cranial lesion and associated suture diastasis observed on CT.

Chronology of the Cerro Esmeralda and Cerro El Plomo individuals

Radiocarbon results indicate that the three individuals are broadly contemporaneous (Table 2), with median calibrated dates of CE 1440, CE 1450, and CE 1480 for CES-A, CES-B, and NEP, respectively. Bayesian credible intervals demonstrate chronological overlap among the dated textile samples associated with the Cerro Esmeralda and Cerro El Plomo individuals (AA-97974, AA-97975, and UGAMS-46589).

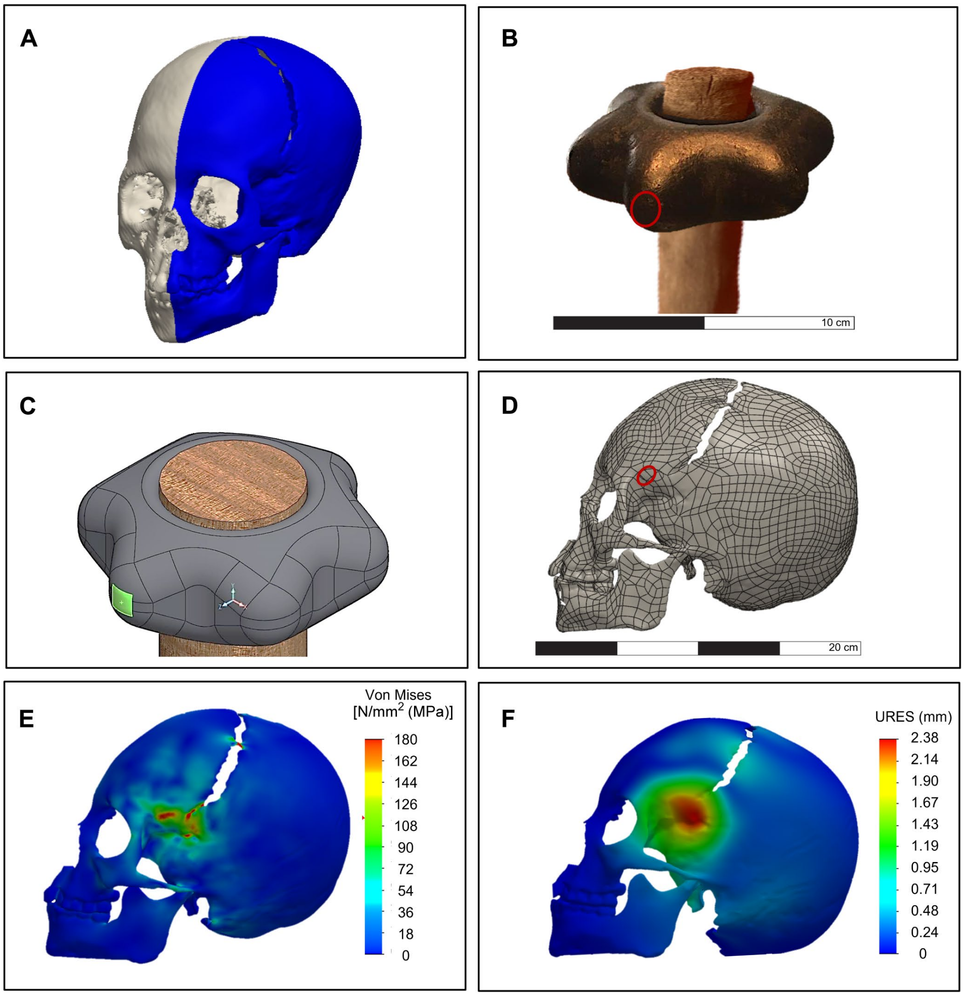

Fig. 5. Finite element model of NEP's skull, proposed Inca weapon, and simulation outputs supporting the biomechanical plausibility of the observed cranial trauma. (**A**) Segmented 3D cranial model used for the simulations; the blue region indicates the solid cranial volume included in the finite element model. (**B**) Star-shaped Inca mace head (scale bar, 10 cm); the circled area indicates the location used to define the contact region. (**C**) 3D model of the star-shaped mace head geometry used to derive the circular 100-mm^2 contact patch (green) applied as the loading area in the simulations. (**D**) CT-derived left hemicranium finite element mesh showing the digitally defined 100-mm^2 impact footprint (circled) used to position the applied load on the left frontotemporal area (scale bar, 20 cm); the mesh was extracted in 3D Slicer and subsequently cleaned in Geomagic Design X. (**E**) von Mises stress (in megapascal) heatmap showing peak concentration at the impact site and stress propagation along the coronal suture. (**F**) Resultant displacement (URES; in millimeters) map showing deformation patterns extending toward the coronal and sagittal sutures.

Table 1. Results from six quasi-static finite element simulations performed in this study to evaluate the biomechanical response of the pediatric cranial model under varying blunt force loads. Values report the maximum tensile stress and deformation at the impact zone, calculated from the simulations and used to assess the mechanical plausibility of fracture initiation.

Force (N)	Tensile max (MPa) in the same point at impact zone	Deformation max (mm)
2500	168	2.18
2600	192	2.27
2700	199	2.35
2800	207	2.44
2900	214	2.53
3000	220	2.62

Radiocarbon dates obtained from human tissues, including bone collagen (UGAMS-54748) and hair (UGAMS-54746), also overlap in their calibrated ranges. With the exception of AA-97975 (CES-B), the calibrated results exhibit multimodal probability distributions. A systematic offset is observed for CES-B and NEP, with textile samples yielding radiocarbon ages ~100 to 160 radiocarbon years before the present (^{14}C yr B.P.) older than the associated human tissues. Within the broader south-central Andean Capacocha record (Table 2), the Cerro Esmeralda and Cerro El Plomo individuals overlap chronologically with Aconcagua [Beta-88785, GX-19991; (*57*, *58*)] but predate Llullaillaco [OxA-14878; (*59*)].

DISCUSSION

Pilgrimage to the Apu

Pilgrimage is widely recognized as a central component of the Capacocha ritual (*2*, *11*, *60*, *61*), yet it has remained difficult to demonstrate archaeologically. Previous isotopic studies of Capacocha individuals have primarily emphasized diet or social status, interpreting isotopic variation as reflecting seasonal changes in maize consumption (*62*, *63*), status-related dietary shifts following selection for sacrifice (*59*), or provisioning through state-sponsored infrastructure such as *tambos* (*64*–*66*). Although these interpretations imply movement, they do not directly test for sustained mobility across ecologically distinct regions.

Sequential isotopic analyses of hair provide a more direct record of late-life movement. The Cerro Esmeralda and Cerro El Plomo individuals exhibit pronounced, directional isotopic changes during the final months of life, documenting distinct life history trajectories (Fig. 2 and table S2). Regime shift analyses identify discrete, statistically significant transitions in isotopic values over time (table S2). The magnitude and persistence of these shifts are inconsistent with short-term dietary fluctuation and instead indicate sustained exposure to different ecological baselines.

Mobility is most clearly expressed in the nitrogen isotope record. Across the Andes, δ^{15}N values in primary producers vary predictably with elevation and precipitation, generally decreasing with increasing moisture and altitude (*67*–*69*). Sustained changes in δ^{15}N values in human tissues therefore reflect movement across these steep environmental gradients. The isotopic trajectories observed here indicate that these individuals moved through regions characterized by markedly different δ^{15}N baselines during the months preceding death. Notably, this environmental signal remains detectable despite the documented use of δ^{15}N-enriched agricultural inputs in parts of the Atacama Desert and the Peruvian Andes (*70*–*72*).

Together, these results provide direct isotopic evidence for prolonged, structured mobility before sacrifice. In the context of Inca ritual practice, the most parsimonious interpretation of this sustained movement is participation in a pilgrimage process involving staged travel across the imperial landscape rather than episodic provisioning or local relocation. Although isotopic data cannot reconstruct specific routes, the convergence of sequential isotopic change, regime shifts, and well-established ecological gradients supports the interpretation of pilgrimage as an embodied and extended component of the Capacocha ritual.

The isotopic records of CES-A and CES-B document contrasting late-life trajectories that ultimately converge during the final stages of the Capacocha ritual. CES-A exhibits a pronounced and directional dietary shift beginning ~9 months before death, marked by increases in δ^{13}C and δ^{15}N values and a concurrent decline in δ^{34}S. Regime shift analyses identify discrete transitions at ~7.5 and ~5.5 months before death, consistent with sustained movement across ecologically distinct regions. The rise in δ^{15}N values suggests displacement from more humid to more arid environments, while the accompanying increase in δ^{13}C, unexpected in arid C_3-dominated settings, indicates increased consumption of C_4 resources, most plausibly maize (*73*). Although Cerro Esmeralda lies within the hyperarid Atacama coastal zone, this δ^{13}C signal likely reflects the intake of agricultural products sourced from interior valleys, where maize cultivation had been established for more than 1500 years. Marine protein consumption is unlikely, as δ^{34}S values remain consistent with a terrestrial dietary signal throughout the final months of life (*74*).

In contrast, CES-B maintains a comparatively stable and specialized dietary profile from ~17 to 3 months before death, with minimal variation in δ^{13}C and δ^{15}N values and no statistically significant regime shifts. Evidence for mobility in this individual is instead captured in the oxygen and hydrogen isotope records, which show increasing δ^{18}O and δ^{2}H values consistent with movement toward the northern Atacama, where meteoric waters are isotopically enriched by evaporation (*75*). The δ^{34}S values likewise support continued reliance on terrestrial resources, while modest increases in δ^{13}C values point to greater intake of inland maize. Notably, during approximately the final month before death, δ^{13}C and δ^{15}N values in CES-B become nearly indistinguishable from those observed in CES-A. This isotopic convergence suggests standardized dietary provisioning during the terminal phase of the ritual process, integrating individuals with distinct prior life histories into a shared ceremonial regime preceding sacrifice.

Together with CES-A and CES-B, the NEP individual documents a third, distinct yet convergent pathway within the broader Capacocha pilgrimage process. NEP exhibits a highly dynamic isotopic profile over the final ~18 months of life, indicating sustained mobility across multiple ecological zones. A progressive decline in $\delta^{15}N$ values reflects movement from arid to more humid environments, while decreasing $\delta^{18}O$ and $\delta^{2}H$ values beginning ~7.5 months before death are consistent with arrival in central Chile. These patterns support a southward trajectory from the Atacama Desert into the Maipo-Mapocho valley, further reinforced by variability in $\delta^{34}S$ values indicative of passage through regions characterized by distinct sulfur baselines. The $\delta^{13}C$ record complements this interpretation: An initial increase between ~18 and 12 months before death suggests increased maize consumption, followed by stabilization and a late decline consistent with a return to C_3-dominated diets or regional isotopic baselines typical of central Chile, where maize and camelids exhibit lower $\delta^{13}C$ and $\delta^{15}N$ values than in northern regions (*76*–*78*). In contrast to the divergent early trajectories observed in CES-A, CES-B, and NEP, all three individuals ultimately converge isotopically during the final months of life. This convergence supports a model of prolonged, multiregional pilgrimage culminating in standardized dietary provisioning during the terminal phase of the Capacocha ritual.

When considered within a broader comparative framework, the patterns documented here align closely with isotopic evidence from other Capacocha individuals, including those from Llullaillaco, Aconcagua, Sara Sara, Chuscha, and Quehuar. Across all individuals analyzed to date, late-life variation is consistently expressed across multiple isotopic systems ($\delta^{13}C$, $\delta^{15}N$, $\delta^{34}S$, $\delta^{18}O$, and $\delta^{2}H$) in the months preceding death (*59*, *62*–*66*). Although the timing, magnitude, and direction of these changes vary, their recurrent presence indicates that dietary and environmental shifts were a widespread feature of the Capacocha process rather than idiosyncratic responses to local conditions. No single isotopic trajectory conforms to a pattern that can be uniquely attributed to elevated social status following selection for sacrifice.

Instead, the temporal structure and diversity of these isotopic changes are more parsimoniously explained by participation in a shared ritual itinerary centered on prolonged pilgrimage. Sustained dietary provisioning during such long-distance journeys would have required systematic support, most plausibly through a combination of state-administered infrastructure (tambos) and ceremonial hosting by local communities. While both mechanisms likely operated in tandem, the isotopic evidence—particularly the late-stage convergence observed among individuals with otherwise distinct life histories—suggests that commensality played a central role. In this model, pilgrims were not merely provisioned but ritually incorporated through shared meals, transforming nourishment into a performative act of affiliation and integration (*79*). These practices would have served both logistical and ideological functions: sustaining participants physically while reinforcing affective, political, and cosmological ties between imperial agents and local populations, thereby contributing to the consolidation of Inca statecraft (*6*, *80*–*83*).

Sacrificial death

Colonial accounts of the Capacocha ritual describe multiple sacrificial practices, including strangulation, asphyxiation, and blunt force trauma (*8*, *12*, *33*, *84*, *85*). These narratives are partly corroborated by archaeological evidence of perimortem injury in several Capacocha contexts, including cranial fractures at Ampato, Sara Sara, and Pichu Pichu; a penetrating wound at Chuscha (*47*, *72*–*74*); and signs interpreted as strangulation at Cerro Esmeralda (*40*). In contrast, other cases, such as the three individuals from Llullaillaco and the El Plomo child, have been interpreted as examples of nonviolent death, attributed to cold exposure or physiological stress at altitude, including hypothermia, hypoxia-related cerebral or pulmonary edema (*49*, *59*, *86*–*90*).

Our reanalysis of the Cerro Esmeralda individuals does not identify conclusive evidence of perimortem violence or lethal cervical trauma. Although strangulation was previously proposed on the basis of external examination and plain radiographs (*40*), the linear marks observed on the neck are superficial and more consistent with textile or garment compression than with ligature marks. CT imaging further demonstrates that the hyoid bones are well preserved, aligned at the expected anatomical level (approximately C3), and without fracture or displacement. Because the hyoid remains partly cartilaginous in juveniles, the absence of bony injury cannot definitively exclude soft tissue neck compression (*91*, *92*); however, the combined external and CT findings do not support the strangulation hypothesis.

More broadly, extensive postrecovery alteration limits diagnostic resolution in both Cerro Esmeralda individuals, particularly CES-B. In CES-A, the right hypochondrial perforation and associated thoracic disruption cannot be evaluated as lethal trauma because the thoracoabdominal organs were removed through the same opening during the 1977 autopsy, and subsequent interventions produced additional incisions and structural loss. CES-B is even more extensively disturbed, showing a systematic autopsy-related incision pattern together with disarticulation and loss of soft tissue, which obscure potential perimortem markers and compromise anatomical integrity. Together, prior interventions, postmortem alterations, and missing anatomical structures hinder definitive attribution of the cause of death.

By contrast, the integration of dermatological/dermatoscopic, histological, tomographic, and biomechanical evidence in the El Plomo child (NEP) supports high-energy blunt force trauma as the most plausible cause of death. External and microscopic examinations reveal intact skin and no evidence of antemortem freezing or cold-induced injury to the extremities, together with an absence of histopathological indicators of inflammation or tissue degeneration. These observations argue against hypothermia as the proximate cause of death. At the same time, the plantar surfaces display marked hyperkeratosis and dark-brown exogenous pigmentation, features unusual for a child of this age, indicating sustained, repeated mechanical loading consistent with prolonged walking over long distances (*54*). In combination with the isotopic evidence for multiregional movement, these findings support an extended pilgrimage trajectory, potentially linking the Cuzco region with the Maipo-Mapocho valley.

The lethal injury is expressed as a left frontal skin lesion directly aligned with an underlying linear perimortem fracture and traumatic diastasis of the coronal and sagittal sutures (Fig. 4). The absence of any reparative bone response, together with limited localized inflammatory change in the overlying soft tissue, is consistent with a perimortem event and a short survival interval. FEAs indicate that an impact load on the order of ~2800 N is sufficient to generate deformation and stress magnitudes compatible with the observed fracture configuration (Fig. 5, E and F, and Table 1), supporting high-energy blunt force trauma as a plausible mechanism. Given the localized

Table 2. Radiocarbon dates for Cerro Esmeralda and Cerro El Plomo individuals and associated materials, with comparative Capacocha dates from Aconcagua and Llullaillaco. Calibrated ages and pooled means are reported as the median (50% quantile) of the 95% credible interval, with 5 to 95% quantiles in brackets; HDRs are listed in adjacent columns.

Material	Lab ID	Percent modern carbon (pMC)	δ13C (‰)	δ15N (‰)	C:N	^{14}C yr B.P.	Calibrated Age (cal CE)	HDR for calibrated age (cal CE)	Pooled mean ^{14}C yr B.P.	Calibrated pooled mean (cal CE)	HDR for calibrated pooled mean (cal CE)	Reference
CES-A												
Textile	AA-97974	93.91 ± 0.4	−20.4			505 ± 34	1440 (1475–1410)	1460–1470 (2.4%), 1460–1400 (92.8%)				This study
CES-B												
Textile	AA-97975	93.5 ± 0.4	−19.9			540 ± 34	1425 (1450–1400)	1450–1400 (92.7%)	485 ± 23	1450 (1475–1430)	1480–1470 (3.3%); 1460–1420 (91.8%)	This study
Bone collagen	UGAMS-54748	94.65 ± 0.24	−12.47	10.54	3.3	440 ± 30	1480 (1610–1450)	1580 (0.4%); 1560–1550 (3.8%); 1620–1580 (8.3%); 1510–1440 (82.5%)				
NEP												
Textile	UGAMS-46589	93.03 ± 0.23	−21.21			580 ± 20	1410 (1430–1340)	1335–1330 (31.3%); 1430–1390 (63.8%)	500 ± 14	1440 (1450–1430)	1450–1430 (88.4%)	This study
Hair	UGAMS-54746	94.93 ± 0.25	−10.57	10.53	3.6	420 ± 20	1490 (1610–1460)	1620–1590 (17.5%); 1510–1450 (77.6%)				This study
Aconcagua												
Hair	Beta-88785					480 ± 40	1450 (1600–1420)	1620–1590 (6%); 1500–1410 (89%)	453 ± 35	1480 (1610–1440)	1560–1550 (2.7%); 1620–1580 (7.2%); 1510–1430 (85.1%)	(*57*)
Bone collagen	GX-19991					370 ± 70	1560 (1740–1460)	1770 (0.4%); 1750 (0.4%); 1795–1780 (1%); 1670–1440 (93.2%)				(*58*)
Llullaillaco												
Hair	OxA-14878					400 ± 25	1535 (1620–1460)	1630–1540 (38.1%); 1510–1450 (57%)				(*59*)

impact focus and the size and geometry of the affected area, the injury is compatible with a compact blunt implement. Among the weapon forms evaluated, a blunt-lobed lithic star-shaped mace provides the closest morphometric concordance with the external lesion (Fig. 5, B and C).

The location, orientation, and geometry of the lesion suggest an obliquely oriented, laterally sweeping impact trajectory across the frontal region. Among the mechanically plausible scenarios, the configuration most consistent with the lesion-fracture alignment involves close-range interaction, with the child oriented toward the assailant and the head flexed downward. However, the precise relative positioning of the individuals cannot be determined from the available evidence (*93*). The impact focus lies in a mechanically vulnerable frontotemporal region near the temporal line, suggesting a deliberately targeted strike rather than an accidental fall. In a juvenile cranium, patent sutures constitute structural weak planes under high-energy loading, with stresses preferentially transmitted and released along these interfaces. Accordingly, the impact energy would have been dissipated through the coronal and sagittal sutures, producing rapid, near-simultaneous cranial failure, as evidenced by the marked sutural diastasis observed on CT (Fig. 4, E to G) (*93*).

Additional observations support a perimortem episode of ritual feeding followed by vomiting. CT imaging shows a dilated esophagus and a stomach filled with food, consistent with ingestion shortly before death as a final ceremonial act. Food residues were also observed on the clothing. Together, these findings indicate vomiting around the time of death, plausibly triggered by acute cranial trauma and rapid physiological collapse. The body was subsequently arranged in a lifelike, sleeping posture, with the injured frontal region positioned against the left knee, suggesting careful postmortem placement within a ceremonial setting. Freezing conditions at high altitude likely contributed to the exceptional preservation of soft tissues.

Together, these results indicate that multiple mechanisms of ritual death were used across Inca Capacocha sites. While some individuals may have died through exposure or altitude-related physiological stressors, others, including the El Plomo child, exhibit evidence consistent with deliberate, high-energy perimortem violence. Despite this diversity, the cases share structured ceremonial preparation and the symbolic incorporation of the body within an imperial ritual framework.

Capacocha ritual in the consecration of the Tawantinsuyu

The Capacocha ceremony was typically performed in response to major events in the life of the Inca Empire. These included natural disasters, the death of an emperor, new investitures or coronations, and the illness of high-ranking authorities (*12*, *32–34*, *94*, *95*). In addition, Capacocha rituals were conducted to commemorate strategic political events, such as the celebration of alliances between the Inca and local leaders (Curacas) (*36*) or to mark the foundational consecration of sacred places (*94*). Multiple circumstances, therefore, could have motivated the performance of these sacrificial rites. The conquest of Collasuyu, the southernmost province of the Tawantinsuyu Empire, is traditionally attributed to Inca Pachacutec around CE 1400 (*94*, *96*, *97*). Radiocarbon chronologies from Capacocha sites reveal a broad temporal range for these sacrifices, spanning the early 15th to the early 16th centuries. Some ceremonies coincide with the initial phases of Inca territorial expansion and political consolidation, whereas others are associated with later periods of imperial control (*98*, *99*).

Radiocarbon dating indicates that CES-A, CES-B, and NEP are broadly contemporaneous, with median calibrated ages in the mid-15th century. Textile samples associated with CES-B and NEP, however, yield radiocarbon ages approximately 100 to 160 ^{14}C years older than those obtained from the corresponding human remains. Several nonmutually exclusive factors may account for this discrepancy. First, textiles may have been produced well before the individual's death. Second, their composite nature—often involving fibers from diverse sources—can introduce chronological variability. Third, some dated materials may not represent truly short-lived samples; for example, ribs typically exhibit a radiocarbon lag of ~13 years due to slower biological turnover (*100*). Fourth, textiles may have functioned as curated heirlooms or may have been deliberately selected for their antiquity, consistent with Andean practices of reusing valued objects across generations (*80*, *101*). These practices would explain why textiles predate the individuals while still retaining ritual relevance.

This interpretation aligns with the ritual logic of Capacocha offerings, in which objects of exceptional quality or symbolic significance were deliberately selected and incorporated into ceremonial contexts (*10*, *80*, *102*). At Cerro El Plomo, the dated artifact is the child's unku—a finely woven garment likely produced for ritual use and curated before its final deposition (*103*). At Cerro Esmeralda, by contrast, the earlier radiocarbon dates derive from tulmas (hair ornaments) within a technically sophisticated textile assemblage interpreted as signaling gendered identity and social distinction (*104–106*). These tulmas secured bifurcated hairstyles formed by multiple twisted locks parted at the crown and gathered into two posterior bundles, a coiffure also depicted in the rear view of female Capacocha figurines commonly discussed as elite representations (*102*, *107*, *108*). Together, these patterns support broader interpretations of Inca offerings as embedded in cosmological, genealogical, and political narratives, in which material objects mediated relationships among human communities, sacred landscapes, and ancestral beings (*10*, *13*, *102*).

This chronological offset highlights the complexity of associating textiles with the precise timing of death but does not alter the conclusion that the sacrifices occurred in the mid-15th century. Instead, it reflects the temporal layering of ritual assemblages, in which both past and present were materially and symbolically integrated. Additional variation may arise from hair samples derived from aggregated segments rather than scalp-proximal strands, potentially introducing temporal averaging (*109*). Despite these sources of variation, textile samples consistently yield calibrated dates with narrower credible intervals and probability distributions that overlap strongly with the highest-density regions (HDRs) of human remains and the pooled mean calibrated age (Table 2). Within a Bayesian framework, this convergence suggests that the offset between textile and bone collagen for CES-B and NEP is minimal and does not compromise the overall chronological coherence of the dataset.

Three additional radiocarbon dates from other Capacocha contexts reveal a broader chronological pattern. Human sacrifices from Llullaillaco and Aconcagua yield calibrated dates ranging between 1420 and 1740 CE (Table 2). These results suggest that Capacocha ceremonies were performed over a prolonged period and at different times across the empire. The radiocarbon ages from Cerro Esmeralda and El Plomo place both sacrifices within the same general chronological horizon as those from Aconcagua yet earlier than Llullaillaco. Notably, the Cerro Esmeralda dates are slightly older than those from Cerro El Plomo, supporting the hypothesis of a gradual southward progression of Capacocha rituals. This pattern is consistent with a broader political expansion originating in southern Peru, beginning with Ampato in the Arequipa region, the earliest known Capacocha of Collasuyu, and extending through northwestern and central western Argentina before reaching northern Chile (*110*, *111*).

The chronology of Inca expansion in Collasuyu remains a subject of ongoing debate, particularly regarding the southern frontier of Tawantinsuyu, in present-day Chile (*110*) and Argentina (*111–115*). It is increasingly evident that the timeline derived from the historical Inca dynasty (*116*) does not fully align with the archaeological record, which frequently indicates earlier dates. Inca expansion appears to have been a complex, multistage process, involving diverse political arrangements. Notably, the circulation of Inca material culture preceded the establishment of effective imperial control by several decades (*117*). Previous chronological modeling suggests that effective integration into Tawantinsuyu may have begun around 1410 CE in the Tarapacá region of northern Chile and as early as 1390 CE in Central Chile (*110*). In Argentina, Bayesian median estimates suggest that provincial incorporation may have begun in the northwest by 1410 CE in Jujuy, followed by Salta, Tucumán, and Catamarca around 1450 CE, and La Rioja, San Juan, and Cuyo, the central-west, around 1440 CE (*111*, *118*). The radiocarbon dates obtained for the Capacocha individuals from Cerro Esmeralda and Cerro El Plomo correspond to a phase of imperial consolidation, postdating earlier evidence of Inca presence in Tarapacá and central Chile (*110*). However, this chronological placement challenges the assumption that Capacocha rituals represent a late phenomenon in the empire's southernmost regions. Instead, these sacrificial acts appeared to have functioned as a continuous political strategy of imperial expansion, sustaining both the symbolic and effective consolidation of Inca authority over newly incorporated communities and territories.

Final comments

In sum, our results demonstrate that pilgrimage, commensality, and sacrifice constituted interlinked Capacocha practices on the western slope of the Andean Cordillera, operating as political and symbolic strategies for integrating newly incorporated territories into the Inca imperial order. Sequential isotopic evidence indicates that the individuals selected for sacrifice undertook extensive ritual journeys. CES-A (Cerro Esmeralda) likely traveled ~900 to 1200 km over ~5 months, while CES-B appears to have covered a comparable distance in roughly 3 months. NEP (Cerro El Plomo) undertook the longest journey, covering an estimated 2600 to 2800 km from Cuzco to the Maipo-Mapocho valley over ~9 months. These routes likely followed interior corridors, where local communities could ritually receive pilgrims and provision them along the way.

NEP exhibits clear evidence of perimortem cranial trauma, whereas the Cerro Esmeralda cases remain etiologically indeterminate. Nonetheless, all three individuals were embedded within ritualized and performative sacrificial contexts. Following death, each individual was carefully arranged and accompanied by multiple offerings and distinctive attire serving as emblems of social and cultural identity (*102*–*108*, *119*). These practices reinforced their role as agents of symbolic transformation and as instruments of Inca statecraft within the ritual landscapes and sacred geographies of Tawantinsuyu.

Our findings further demonstrate that Capacocha rituals were conducted in the southernmost regions of Tawantinsuyu during the consolidation of Inca expansion. Their earlier-than-expected chronological placement challenges the assumption that these ceremonies necessarily depended on, or followed, the full establishment of military control. Instead, these rites appear to have operated as strategic instruments for consecrating Inca authority and asserting sovereignty in newly incorporated territories. The state's regulation of the movement, nourishment, and deaths of sacrificial individuals reflects a profound exercise of biopolitical power (*18*) and reinforces the interpretation of Capacocha sites as persistent places within imperial landscapes (*17*). Through Capacocha, sacrificial children were transformed into ritual emissaries of their communities (ayllus) in the presence of the apus, materially mediating relationships between human collectives and powerful mountain beings (*8*, *61*, *120*). Within this framework, the body, attire, and accompanying offerings did not merely "feed" the mountains but enacted a sanctioned transfer of vitality and representation, embedding local communities within an imperial-sacred geography (*10*, *120*). This study deepens our understanding of the sociopolitical and religious dimensions of Capacocha and its ritual entanglements within ancient Andean traditions. Last, our multidisciplinary approach underscores the value of integrating isotopic, forensic, and archaeological lines of evidence to reconstruct the sequencing, mechanisms, and broader social logics of these complex ceremonial events.

MATERIALS AND METHODS

Sequential stable isotope analyses of hair strands

We performed multielement stable isotope analyses ($\delta^{13}C$, $\delta^{15}N$, $\delta^{34}S$, $\delta^{18}O$, and $\delta^{2}H$) along scalp hair to track isotopic variation linked to life history change, with emphasis on dietary shifts during pilgrimage. We conducted sequential analyses for three individuals and tailored sampling to preservation. We collected hair from CES-A (780 mg) and CES-B (1360 mg) at the root in the nuchal region; for the El Plomo child (NEP), we cut hair (360 mg) with surgical scissors as close to the scalp as possible because the hair had been frozen to prevent damage.

Hair sample preparation was carried out at the Department of Human Evolution, Max Planck Institute for Evolutionary Anthropology (MPI-EVA, Leipzig, Germany), following O'Connell *et al.* (*121*). Multiple hairs per individual were aligned to match identical growth periods and cut into serial segments (5 mm: CES-A, 14 samples; CES-B, 34 samples; 15 mm: NEP, 12 samples from the proximal end). All segments were analyzed in duplicate; ~0.5 mg was weighed into tin capsules for $\delta^{13}C$ and $\delta^{15}N$, and into tin capsules containing 3 mg of vanadium pentoxide for $\delta^{34}S$.

At the MPI-EVA, we analyzed $\delta^{13}C$ and $\delta^{15}N$ for CES-A and CES-B using a Delta XP continuous-flow isotope ratio mass spectrometer (Thermo-Finnigan, Bremen, Germany) coupled to a Flash EA 2112 elemental analyzer. We calibrated measurements using working standards, including EVA-0009 methionine ($\delta^{15}N\_AIR = +7.26‰$; $\delta^{13}C\_VPDB = -20.80‰$), International Atomic Energy Agency (IAEA) N1/CH ($\delta^{15}N\_AIR = +15.44‰$; $\delta^{13}C\_VPDB = -12.22‰$), and liver 1577b ($\delta^{15}N\_AIR = +11.88‰$; $\delta^{13}C\_VPDB = -27.22‰$). At the Stable Light Isotope Facility (University of Bradford), we measured $\delta^{13}C$, $\delta^{15}N$, and $\delta^{34}S$ for NEP, as well as $\delta^{34}S$ for CES-A and CES-B, using a Flash EA 1112 elemental analyzer coupled to a Thermo Finnigan Delta Plus XL isotope ratio mass spectrometer via a Conflo III interface. We calibrated $\delta^{13}C$ and $\delta^{15}N$ using fish gelatin ($\delta^{15}N\_AIR = +14.45‰$; $\delta^{13}C\_VPDB = -15.52‰$) and methionine ($\delta^{15}N\_AIR = -3.0‰$; $\delta^{13}C\_VPDB = -26.6‰$) as working standards, both calibrated against the caffeine IAEA-600 international standard ($\delta^{15}N\_AIR = +1‰$; $\delta^{13}C\_VPDB = -27.77‰$). For sulfur, we calibrated $\delta^{34}S$ using methionine ($\delta^{34}S\_VCDT = +12.6‰$) together with international standards: silver sulfide IAEA-S1 ($\delta^{34}S\_VCDT = -0.30‰$), IAEA-S2 ($\delta^{34}S\_VCDT = +22.62‰$), and barium sulfate IAEA-NBS127 ($\delta^{34}S\_VCDT = +21.1‰$). We achieved an analytical precision of $\pm 0.20‰$ for $\delta^{13}C$ and $\delta^{15}N$ and $\pm$ 0.4‰ for $\delta^{34}S$ measurements. We report $\delta^{13}C$, $\delta^{15}N$, and $\delta^{34}S$ values relative to Vienna Pee Dee Belemnite (VPDB), air, and Vienna Canyon Diablo Troilite (VCDT), respectively. Although the atomic C:N ratio of keratin is not generally considered a strong indicator of preservation, all sequential hair samples yielded C:N atomic ratios within the accepted range for well-preserved human hair keratin proposed by O'Connell *et al.* (*121*) (table S1).

For oxygen and hydrogen stable isotope determinations, we prepared hair samples from CES-B and NEP by carefully separating, aligning, and trimming fibers of comparable lengths to obtain ~1 mg of material per sample. For NEP, we segmented approximately 19 fibers (≥11 cm each) into 1-cm lengths and weighed them at the University of Bradford. We prepared CES-B following the same protocol, using approximately 15 fibers (≥18 cm each). We equilibrated all samples under laboratory humidity for 14 days and then oven-dried them at 60°C for 7 days. We measured $\delta^{18}O$ and $\delta^{2}H$ values in hair segments at the University of Bradford using a Europa Scientific elemental analyzer coupled to isotope ratio mass spectrometry. We normalized results to Vienna Standard Mean Ocean Water (VSMOW) through repeated analyses of working standards: oxygen IA-R006 (cane sugar; $\delta^{18}O\_VSMOW = +35.23‰$) and hydrogen IA-R002 (mineral oil; $\delta^{2}H\_VSMOW = -111.2‰$). We tested accuracy using quality control standards, including sucrose (IAEA-CH-6; $\delta^{18}O$_VSMOW = +36.40‰) and cellulose (IAEA-CH-3; $\delta^{18}O$_VSMOW = +32.20‰) for oxygen and IA-R002 and IA-R072 (pump oil; $\delta^{2}H$_VSMOW = −148.6‰) for hydrogen. To further validate $\delta^{18}O$ and $\delta^{2}H$ measurements, we analyzed nonexchangeable hydrogen standards USGS42 ($\delta^{2}H$_VSMOW = −72.9‰; $\delta^{18}O$_VSMOW = +8.56‰), USGS43 ($\delta^{2}H$_VSMOW = −44.4‰; $\delta^{18}O$_VSMOW = +14.11‰), USGS CBS ($\delta^{2}H$_VSMOW = −157.0‰; $\delta^{18}O$_VSMOW = +2.39‰), and USGS KHS ($\delta^{2}H$_VSMOW = −35.3‰; $\delta^{18}O$_VSMOW = +21.21‰) alongside the hair samples. Analytical precision was ±0.2‰ for both isotopes.

Regime shifts

To identify periods of structural shifts in the life trajectory of each individual, we applied the sequential *t* test algorithm (*122*) to detect changes in the mean stable isotope values across sequential segments of hair samples. Raw stable isotope data were minimum–maximum normalized to a 1-0 scale for standardization (table S1). A cutoff length (*l*) of 3 consecutive data points (i.e., three hair sections) was used to avoid detecting shifts caused by noise. This choice aligns with the sequential *t* test's design to identify abrupt, rather than gradual, changes in the mean (*122*). Shorter cutoff lengths are more effective for capturing significant differences between consecutive periods. A significance threshold (*P*) of 0.05 was set to identify statistically significant regime shifts, and a Huber weight parameter of 2 was applied to manage outliers. Regime shifts were identified using the RSI, which quantifies deviations from the expected mean of a new regime. A shift was declared (or rejected) if the RSI remained positive (or negative) over the entire cutoff length. We further explored regime shifts in the compounded stable isotopic signature across hair segments, providing integrated insights into changes in dietary patterns over time. Specifically, we generated a stable isotopic change index by aggregating sequential min-max values (*123*) for isotopic signatures from each hair segment, with most indices calculated between equally spaced stable isotope pairs to ensure consistent resolution. For example, a C-N index was calculated for CES-A (0.5 to 11.5 cm) and NEP (1.5 to 16.5 cm), while an O-H index was computed for CES-B (1.0 to 17.0 cm) and NEP (1.5 to 12 cm). In addition, for CES-B, a carbon-nitrogen-sulfur index was derived. Regime shift analyses were conducted using the same modeling decisions and conditions as outlined previously. All regime shift analyses were conducted using the SRSD v.3.2 package for Excel (*122*, *124*).

CT scan

We acquired multislice CT images for this study. We scanned the Cerro Esmeralda bodies using a Toshiba Asteion 4 system (Toshiba Medical Systems Corporation) with a 512 × 512 matrix, 120 kV, 60 mAs, and 1.5-mm slice thickness. We scanned the Cerro El Plomo child using a Siemens Somatom Definition AS 128 scanner (Siemens, Erlangen, Germany) with a 512 × 512 matrix, 120 kV, 300 mAs, and 0.6-mm slice thickness. We reviewed the images and conducted the medical assessment on a dedicated diagnostic workstation with high-resolution monitors using the AGFA Enterprise Imaging PACS platform (Agfa Healthcare, Mortsel, Belgium). We examined CT datasets on axial series and multiplanar reconstructions using soft tissue and bone-optimized kernels. To facilitate visualization of cranial lesions, we used cinematic surface-shaded display postprocessing and applied curved planar reformation in OsiriX v13.0.

To inform interpretation of the NEP cranial injury, we analyzed CT datasets in OsiriX v13.0 to obtain quantitative measurements of the external skin lesion (dimensions and orientation) and to assess its spatial correspondence with the underlying fracture morphology on bone reconstructions. We also inspected and measured CT-derived 3D surface renderings in MeshLab [Visual Computing Laboratory, Institute of Information Science and Technologies, Italian National Research Council (ISTI-CNR)] for geometric comparisons. On the basis of lesion geometry and orientation, we evaluated candidate blunt force weapon types through a digital geometric compatibility assessment using 3D weapon models hosted on Sketchfab (e.g., model ID 6Woo7). We considered four implement types: a round stone mace head, stone star-shaped mace heads with blunt versus angular lobes, and a metal star-shaped mace head with angular lobes. We measured contact geometry (maximum length/width, outline, and edge characteristics) digitally in MeshLab and compared it with the lesion footprint to define the modeled impact area used in the finite element simulations described below (Fig. 5, A to D).

Modeling blunt trauma

To assess the biomechanical plausibility of the cranial lesion observed in NEP, we carried out a CT-based 3D reconstruction and FEA. We segmented the CT data in 3D Slicer v5.0.3 (*125*, *126*) using a Hounsfield unit threshold range of 37 to 3057. We then manually refined the segmentation in the "Segment Editor" module to preserve anatomical fidelity and exported the segmented volume as a surface mesh using the "Export visible segment to models" function.

We imported the mesh into Geomagic Design X 2020 (3D Systems Corporation, SC, USA) and isolated the region of interest as a half-skull (hemicranium) model corresponding to the left superior cranial portion that includes the impact area, followed by cleaning and smoothing (Fig. 5, A to D). Next, we transferred the processed surface to SolidWorks 2022 (Dassault Systèmes, MA, USA) to generate a closed solid model. The resulting solid had a mass of 0.119222 kg, a volume of 0.000119217 m^3, and a density of 1000.04 kg/m^3, which yields a calculated weight of 1.16838 N.

We performed FEA in SolidWorks Simulation using both linear (quasi-static) and nonlinear dynamic solvers. We implemented six quasi-static loading conditions (Table 1) to quantify tensile stress and deformation at the impact focus. We applied loads spanning 2500 to 3000 N over a 100-mm^2 contact area, chosen to approximate the footprint of a compact blunt implement consistent with a star-shaped Inca mace (Fig. 5, B to D). We defined boundary conditions by constraining translational degrees of freedom to approximate cranial fixation relative to the surrounding anatomical context.

To represent sutural opening in a juvenile cranium, we modeled the coronal and sagittal sutures as compliant interfaces by implementing an integrated hinge connector approach along the sutural paths (hinge-type connectors permitting relative rotation/opening while restricting rigid body translation). This configuration allowed us to evaluate stress transmission toward sutures and the propensity for diastasis under high-energy loading.

We defined material behavior in SolidWorks as a linear elastic, isotropic model with a Mohr-Coulomb failure criterion. We assigned material properties to approximate juvenile cranial cortical bone: Young's modulus E = 7000 MPa (*127*), Poisson's ratio ν = 0.22, shear modulus G = 2320 MPa, and density ρ = 1000 kg/m^3 (*128*). We specified strength parameters as a tensile limit of 90 MPa (*129*), a compressive limit of 10,800 MPa, and a yield stress of 114 MPa

(*55*, *56*). We ran all simulations at 298 K (25°C). From the CT data, we measured local cranial thickness at the impact focus (2.448 mm) and used this value as a reference for interpreting modeled deformation. On the basis of the quasi-static simulations, we selected the 2800 N load case for nonlinear dynamic analysis because it produced deformation comparable to the measured thickness and generated stress magnitudes consistent with tensile failure. We then used the nonlinear dynamic model to evaluate time-dependent stress propagation and the potential for mesh rupture in the impact zone (Fig. 5, E and F).

Last, we used the 2800 N load case to estimate an equivalent impact velocity using Newton's second law under a simplified loading approximation; we report this estimate in movie S1 and compare it with velocities reported in forensic blunt trauma experiments using flat and cylindrical impactors (*52*). We designed this modeling framework to evaluate mechanical plausibility rather than reconstruct the exact event, posture, object velocity, or behavioral context. Accordingly, we did not incorporate soft tissues, textile layers, or cranial viscoelasticity, which represent acknowledged limitations of the approach.

Chronology

We established the chronology for the three bodies by conducting five accelerator mass spectrometry (AMS) radiocarbon dating on textiles and bone collagen (Table 2). For both bodies from Esmeralda, we sampled textiles from the tulmas (pompons of the headdress; Fig. 3, G and H). In addition, a radiocarbon dating analysis was conducted on bone collagen extracted from a fragmented rib for CES-B. For the El Plomo child, a textile fiber was extracted from the red *Huariro* (fringes; fig. S2A) of the unku (tunic) he wore, along with a small hair sample taken from one of the braids at the nape of his neck. Sample preparation and analyses were conducted at the Center for Applied Isotope Studies at the University of Georgia and the AMS Laboratory at the University of Arizona. The calibration of all ^{14}C dates presented here was performed using the calibration curve SHCAL20 (*130*) in the Bayesian radiocarbon chronology package Bchron 4.7.6 (*131*) for R. The median calibrated age is reported as the 50% quantile of the 95% credible interval, with the 5 and 95% quantiles also provided in calibrated Common Era. We also extracted the 95% highest posterior density regions (HDR) for each calibrated age (table S5). When two radiocarbon dates were available for a given mummy, they were combined using the pooled mean tool in CALIB 8.0 (*132*), and the resulting value was subsequently calibrated as outlined above.

Ethical consideration

We conducted this study in accordance with applicable ethical and legal regulations for research on archaeological human remains in Chile, under the FAIP-N-43-INV project of the Servicio Nacional del Patrimonio Cultural. Ethical approval was granted by the Comité de Ética en la Investigación of the Servicio Nacional del Patrimonio Cultural de Chile (https://investigacion.patrimoniocultural.gob.cl/comite-de-etica-en-la-investigacion), which oversees research involving human remains from museum collections and archaeological contexts. We prioritized nondestructive approaches and minimized sampling to preserve the integrity of these exceptional individuals. We also support transparency and ethical responsibility through community engagement and public scientific outreach.

Supplementary Materials

The PDF file includes:
Provenance statement
Figs. S1 and S2
Tables S1 and S2
Legend for movie S1
Legend for data S1

Other Supplementary Material for this manuscript includes the following:
Movie S1
Data S1

REFERENCES

1. E. P. Benson, A. G. Cook, *Ritual Sacrifice in Ancient Peru* (University of Texas Press, 2001).
2. T. Besom, *Inka Human Sacrifice and Mountain Worship: Strategies for Empire* (University of New Mexico Press, 2013).
3. D. Carrasco, "Sacrifice/human sacrifice in religious traditions," in *The Oxford Handbook of Religion and Violence* (Oxford Univ. Press, 2013), pp. 209–225.
4. T. Insoll, *The Oxford Handbook of the Archaeology of Ritual and Religion* (Oxford Univ. Press, 2011).
5. H. D. Klaus, J. M. Toyne, "Chapter one ritual violence on the North Coast of Peru: Perspectives and prospects in the archaeology of ancient Andean sacrifice," in *Reconstructing Sacrifice on the North Coast of Peru*, H. D. Klaus, J. M. Toyne, Eds. (University of Texas Press, 2016), pp. 1–24.
6. P. Gose, *Invaders as Ancestors* (University of Toronto Press, 2008).
7. T. Bray, "Ritual commensality between human and non-human persons. Investigating native ontologies in the late pre-Columbian Andean world," in *Between Feasts and Daily Meals. Towards an Archaeology of Commensal Spaces*, S. Pollock, Ed. (EditionTopoi, 2015), pp. 225–241.
8. J. Reinhard, *The Ice Maiden - Inca Mummies & Sacred Sites* (National Geographic Society, 2006).
9. M. C. Ceruti, Elegidos de los dioses: Identidad y estatus en las víctimas sacrificiales del volcán Llullaillaco. *Boletín De Arqueología PUCP* , 263–275 (2003). [Chosen of the Gods: Identity and Status in the Sacrificial Victims of Llullaillaco Volcano].
10. P. Duviols, La Capacocha: Mecanismo y función del sacrificio humano, su proyección geométrica, su papel en la política integracionista y en la economía redistributiva del Tawantinsuyu. *Allpanchis* **8**, 11–57 (1976). [The Capacocha: Mechanism and Function of Human Sacrifice, Its Geometric Projection, Its Role in Integrationist Politics and in the Redistributive Economy of Tawantinsuyu].
11. M. Rostworowski, Peregrinaciones y procesiones rituales en los Andes. *J. Soc. Am.* **89**, 97–123 (2003). [Pilgrimages and Ritual Processions in the Andes].
12. M. de Murua, "Historia del origen y genealogia real de los reyes yngas del Piru. De sus hechos, costumbres, trajes, y manera de gobierno," in *Códice Murúa 1590*, J. Ossio Acuña, Ed. (Testimonio, 2004), vol. II. [History of the Origin and Royal Genealogy of the Inca Kings of Peru: Their Deeds, Customs, Dress, and Form of Government].
13. J. Reinhard, C. Ceruti, *Inca Rituals & Sacred Mountains: A Study of the World's Highest Archaeological Sites* (Cotsen Institute of Archaeology Press, 2010).
14. A. A. Ferrari, F. A. Acuto, I. Leibowicz, J. Izaguirre, C. Jacob, Pilgrimage, mountain worshiping, and human–non-human entities' interactions in the South Andes: A case study from the North Calchaquí Valley (Salta, Argentina). *J. Anthropol. Archaeol.* **61**, 101266 (2021).
15. F. Acuto, "Sacred geography, Wak'as, and Inka colonialism in the Southern Andes," in *Rethinking the Inca*, F. M. Hayashida, A. Troncoso, D. Salazar, Eds. (University of Texas Press, 2022), pp. 13–34.
16. T. Saintenoy, Sur le chemin d'Apurimaq. *L'Homme* , 7–33 (2013). [On the Apurimaq Road].
17. B. J. Skousen, C. B. Antoniuk, Rethinking persistent places: Relationships, affects, and atmospheres. *J. Archaeol. Method Theory* **33**, 10.1007/s10816-025-09743-3 (2026).
18. E. R. Swenson, "Sacrificial landscapes and the anatomy of Moche biopolitics," in *Powerful Places in the Ancient Andes*, J. Jennings, E. R. Swenson, Eds. (The University of New Mexico Press, 2013), pp. 247–286.
19. F. A. Acuto, I. Leibowicz, In pursuit of the sacred: Understanding Inka colonialism in the Andes. *Comparativ* **30**, 313–326 (2020).
20. E. Arkush, C. Stanish, Interpreting Conflict in the Ancient Andes. *Curr. Anthropol.* **46**, 3–28 (2005).
21. B. Sillar, Caminando a través del tiempo: geografías sagradas en Cacha/Raqchi, departamento del Cuzco (Peru). *Rev. Andin.* **35**, 221–246 (2002). [Walking Through Time: Sacred Geographies in Cacha/Raqchi, Department of Cuzco, Peru].
22. B. S. Bauer, C. Stanish, Ritual and pilgrimage in the ancient Andes: The island of the Sun and the Moon. *J. Lat. Am. Stud.* **35**, 897–898 (2003).
23. P. Eeckhout, Relatos míticos y prácticas rituales en Pachacamac. *Bull. Inst. Fr. Études Andines* **33**, 1–54 (2004). [Myths and Ritual Practices at Pachacamac].

24. P. Eeckhout, "El oráculo de Pachacamac y los peregrinajes a larga distancia en el mundo andino antiguo," in *Adivinación y Oráculos En El Mundo Andino Antiguo* (Pontificia Universidad Católica del Perú, 2008), pp. 161–180. [The Oracle of Pachacamac and Long-Distance Pilgrimages in the Ancient Andean World].
25. B. S. Bauer, C. Stanish, *Ritual and Pilgrimage in the Ancient Andes: The Islands of the Sun and the Moon* (University of Texas Press, 2001).
26. J. B. Skousen, Rethinking archaeologies of pilgrimage. *J. Soc. Archaeol.* **18**, 261–283 (2018).
27. C. Dávila, "Peregrinaciones y Oráculos en el imperio Inca: La política de la religión," thesis, Pontificia Universidad Católica del Perú, Lima (2022). [Pilgrimages and Oracles in the Inca Empire: The Politics of Religion].
28. M. Dietler, "Theorizing the feast: Rituals of consumption, commensal politics and power in African contexts," in *Feasts: Archeological and Ethnographic Perspectives on Food, Politics and Power*, M. Dietler, B. Hayden, Eds. (Smithsonian Institution Press, 2001), pp. 65–114.
29. T. Bray, Ritual commensality between human and non-human persons: Investigating native ontologies in the late pre-Columbian Andean world. *eTopoi J. Anc. Stud., Spec.* **2**, 197–212 (2012).
30. E. Swenson, J. Jennings, "Introduction: Place, landscape, and power in the Ancient Andes," in *Powerful Places in the Ancient Andes*, J. Jennings, E. Swenson, Eds. (University of New Mexico Press, 2018), pp. 1–54.
31. P. Mignone, Ritualidad estatal, Capacocha y actores sociales locales: El Cementerio del volcán Llullaillaco. *Estud. Atacam.* , 43–62 (2010). [State Rituality, Capacocha, and Local Social Actors: The Cemetery of Llullaillaco Volcano].
32. P. Sarmiento de Gamboa, *Historia de Los Incas [1570-1575]* (Miraguano Ediciones, 2013). [The History of the Incas].
33. B. Cobo, *Inca Religion and Customs [1623]* (University of Texas Press, Austin, 1990).
34. C. de Molina, *Relación de las fábulas y ritos de los incas* [1575], J. Calvo-Pérez, H. Urbano, Eds., Biblioteca de Estudios Coloniales, vol. 7 (Cátedra UNESCO Cultura, Turismo, Desarrollo, 2008). [Account of the Fables and Rites of the Incas].
35. T. Besom, *Of Summits and Sacrifice* (University of Texas Press, 2009); http://jstor.org/stable/10.7560/719774.
36. R. Hernández Príncipe, Mitología Andina. *Inca* **1**, 25–78 (1923).
37. A. Ferrari, J. Izaguirre, I. Leibowicz, F. Acuto, M. Tello, Geografías locales y escenografías imperiales. *Estud. Atacameños* **71**, e6284 (2025). [Local Geographies and Imperial Scenographies].
38. I. Leibowicz, R. Moyano, A. Ferrari, F. Acuto, C. Jacob, Culto y Peregrinaje Inka en el Nevado de Cachi, Salta, Argentina. Nuevos datos en Arqueología de Alta Montaña. *Ñawpa Pacha* **38**, 183–202 (2018). [Inka Worship and Pilgrimage on Nevado de Cachi, Salta, Argentina: New Data in High-Mountain Archaeology].
39. J. Kantner, K. J. Vaughn, Pilgrimage as costly signal: Religiously motivated cooperation in Chaco and Nasca. *J. Anthropol. Archaeol.* **31**, 66–82 (2012).
40. J. Checura, Funebria incaica en el cerro Esmeralda (Iquique, I Región). *Estud. Atacameños* , 125–141 (1977).
41. D. Ubelaker, Hyoid fracture and strangulation. *J. Forensic Sci.* **37**, 1216–1222 (1992).
42. F. Niort, Y. Godio-Raboutet, R. Torrents, P. Adalian, G. Léonetti, M.-D. Piercecchi-Marti, L. Thollon, Transmission of force to the hyoid bone during manual strangulation: Simulation using finite element numerical models. *Forensic Sci. Int.* **257**, 420–424 (2015).
43. P. Saukko, B. Knight, *Knight's Forensic Pathology* (CRC Press, ed. 4, 2024).
44. A. M. Malek, R. T. Higashida, V. V. Halbach, C. F. Dowd, C. C. Phatouros, T. E. Lempert, P. M. Meyers, W. S. Smith, R. Stoney, Patient presentation, angiographic features, and treatment of strangulation-induced dissection of the internal carotid artery. *J. Neurosurg.* **92**, 481–487 (2000).
45. B. Schrag, P. Vaucher, M. D. Bollmann, P. Mangin, Death caused by cardioinhibitory reflex cardiac arrest—A systematic review of cases. *Forensic Sci. Int.* **207**, 77–83 (2011).
46. H. M. de Bakker, M. V. Warmbrunn, P. van den Biggelaar, V. Soerdjbalie-Maikoe, B. S. de Bakker, Fracture patterns of the hyoid-larynx complex after fatal trauma on the neck: Retrospective radiological postmortem analysis of 284 cases. *Int. J. Leg. Med.* **134**, 1465–1473 (2020).
47. A. Gupta, A. Kohli, N. K. Aggarwal, K. K. Banerjee, Study of age of fusion of hyoid bone. *Leg. Med.* **10**, 253–256 (2008).
48. D. H. D'Souza, S. S. Harish, J. Kiran, Fusion in the hyoid bone: Usefulness and implications. *Med. Sci. Law* **50**, 197–199 (2010).
49. G. Mostny, La Momia del Cerro El Plomo. *Bol. Mus. Nac. Hist. Nat.* **27**, 9–13 (1959).
50. J.-S. Raul, C. Deck, F. Meyer, A. Geraut, R. Willinger, B. Ludes, A finite element model investigation of gunshot injury. *Int. J. Leg. Med.* **121**, 143–146 (2007).
51. R. I. Matoso, A. R. Freire, L. S. de Mello Santos, E. D. Junior, A. C. Rossi, F. B. Prado, Comparison of gunshot entrance morphologies caused by .40-caliber Smith & Wesson, .380-caliber, and 9-mm Luger bullets: A finite element analysis study. *PLOS ONE* **9**, e111192 (2014).
52. D. Sahoo, C. Deck, N. Yoganandan, R. Willinger, Influence of stiffness and shape of contact surface on skull fractures and biomechanical metrics of the human head of different population under lateral impacts. *Accid. Anal. Prev.* **80**, 97–105 (2015).
53. D. Sahoo, C. Deck, N. Yoganandan, R. Willinger, Development of skull fracture criterion based on real-world head trauma simulations using finite element head model. *J. Mech. Behav. Biomed. Mater.* **57**, 24–41 (2016).
54. V. Catalán, M. Castro, R. Cabrera, V. Silva-Pinto, A. Castro, C. Lecaros, Paleodermatology: Dermatoscopic findings of "Niño del Plomo" an Incan mummy in Chile. *JAAD Case Rep.* **42**, 74–77 (2023).
55. J. Currey, "Chapter A1 cortical bone," in *Handbook of Biomaterial Properties* (Springer New York, 2016), pp. 3–13.
56. M. Kutz, *Standard Handbook of Biomedical Engineering and Design* (McGraw-Hill Education, Revised Edition, 2003); https://www.accessengineeringlibrary.com/content/book/9780071356374.
57. J. R. Bárcena, *Arqueología de Mendoza: Las dataciones absolutas y sus alcances* (EDIUNC, 1998). [Archaeology of Mendoza: Absolute Dates and Their Scope].
58. J. Schobinger, "Datación radiocarbónica de la momia del Aconcagua por el Laboratorio Geochron," in *El Santuario Incaico Del Cerro Aconcagua*, J. Schobinger, Ed. (EDIUNC, 2001), pp. 173–177. [Radiocarbon Dating of the Aconcagua Mummy by the Geochron Laboratory].
59. A. S. Wilson, T. Taylor, M. C. Ceruti, J. A. Chavez, J. Reinhard, V. Grimes, W. Meier-Augenstein, L. Cartmell, B. Stern, M. P. Richards, M. Worobey, I. Barnes, M. T. P. Gilbert, Stable isotope and DNA evidence for ritual sequences in Inca child sacrifice. *Proc. Natl. Acad. Sci. U.S.A.* **104**, 16456–16461 (2007).
60. M. de Murúa, *Historia General Del Perú* (Bibliotheca Americana Vetus, Joyas Bibliográficas., 1964), vol. 2. [General History of Peru].
61. M. C. Ceruti, *Llullaillaco: Sacrificios y ofrendas en un santuario inca de alta montaña/ Llullaillaco: Sacrifices and Offerings on a High Mountain Inca Shrine* (Ediciones Universidad Católica de Salta, 2003).
62. J. Fernández, H. O. Panarello, J. Schobinger, The Inka mummy from Mount Aconcagua: Decoding the geographic origin of the "Messenger to the Deities" by means of stable carbon, nitrogen, and sulfur isotope analysis. *Geoarchaeology* **14**, 27–46 (1999).
63. Z. D. Sharp, V. Atudorei, H. O. Panarello, J. Fernández, C. Douthitt, Hydrogen isotope systematics of hair: Archeological and forensic applications. *J. Archaeol. Sci.* **30**, 1709–1716 (2003).
64. V. A. Killian Galván, A. Tessone, L. O. Valenzuela, Z. D. Sharp, H. O. Panarello, Stable isotope analysis of the Inca mummy from Nevado de Chuscha (Salta, Argentina)*. *Archaeometry* **62**, 19–34 (2020).
65. V. A. Killian Galván, C. N. Collado, R. F. Heras, M. F. Zigarán, G. R. Browning, V. Seldes, Análisis isotópico seriado de una muestra de cabello del individuo inhumado en el volcán Quehuar (Salta, Argentina). *Ñawpa Pacha* **44**, 51–68 (2024).
66. E. Poullallion, V. A. Killian Galván, V. Seldes, M. F. Zigarán, G. Recagno Browning, F. Fourel, T. Clauzel, J.-P. Flandrois, N. Séon, L. Simon, R. Amiot, C. Lécuyer, The Inca child of the Quehuar volcano: Stable isotopes clue to geographic origin and seasonal diet, with putative seaweed consumption. *J. Archaeol. Sci. Rep.* **59**, 104784 (2024).
67. J. Houston, Variability of precipitation in the Atacama Desert: Its causes and hydrological impact. *Int. J. Climatol.* **26**, 2181–2198 (2006).
68. F. P. Díaz, M. Frugone, R. A. Gutiérrez, C. Latorre, Nitrogen cycling in an extreme hyperarid environment inferred from δ15N analyses of plants, soils and herbivore diet. *Sci. Rep.* **6**, 22226 (2016).
69. L. L. Tieszen, M. Chapman, Dietary reconstruction based on carbon, nitrogen, and sulfur stable isotopes in the Atacama Desert, Northern Chile. *Actas del I Congreso Internacional de Estudios sobre Momias* **1**, 409–425 (1992).
70. F. Santana-Sagredo, R. J. Schulting, P. Méndez-Quiros, A. Vidal-Elgueta, M. Uribe, R. Loyola, A. Maturana-Fernández, F. P. Díaz, C. Latorre, V. B. McRostie, C. M. Santoro, V. Mandakovic, C. Harrod, J. Lee-Thorp, 'White gold' guano fertilizer drove agricultural intensification in the Atacama Desert from ad 1000. *Nat. Plants* **7**, 152–158 (2021).
71. P. Szpak, C. D. White, F. J. Longstaffe, J.-F. Millaire, V. F. V. Sánchez, Carbon and nitrogen isotopic survey of Northern Peruvian plants: Baselines for paleodietary and paleoecological studies. *PLOS ONE* **8**, e53763 (2013).
72. P. Szpak, F. J. Longstaffe, J.-F. Millaire, C. D. White, Stable isotope biogeochemistry of seabird guano fertilization: Results from growth chamber studies with maize (Zea Mays). *PLOS ONE* **7**, e33741 (2012).
73. E. M. Gayo, T. Martens, H. Stuart-Williams, J. Fenner, C. M. Santoro, C. Carter, J. Cameron, Procurement of camelid fiber in the hyperarid Atacama Desert coast: Insights from stable isotopes. *Quat. Int.* **548**, 71–83 (2020).
74. K. Rodiouchkina, I. Rodushkin, S. Goderis, F. Vanhaecke, Longitudinal isotope ratio variations in human hair and nails. *Sci. Total Environ.* **808**, 152059 (2022).
75. M. R. Buzon, C. A. Conlee, G. J. Bowen, Refining oxygen isotope analysis in the Nasca region of Peru: An investigation of water sources and archaeological samples. *Int. J. Osteoarchaeol.* **21**, 446–455 (2011).
76. F. Falabella, M. T. Planella, R. H. Tykot, El Maíz (Zea Mays) en el Mundo Prehispánico de Chile Central. *Lat. Am. Antiq.* **19**, 25–46 (2008). [Maize (Zea mays) in the Prehispanic World of Central Chile].

77. F. Falabella, L. Sanhueza, V. Abarca, M. J. Herrera, Social differentiation in the pre-Hispanic horticultural societies of central Chile (200–1500 AD). A stable isotope study. *Quat. Int.* **548**, 41–56 (2020).
78. F. Falabella, M. T. Planella, E. Aspillaga, L. Sanhueza, R. H. Tykot, Dieta en sociedades alfareras de Chile Central: Aporte de análisis de isótopos estables. *Chungara* **39**, 5–27 (2007). [Diet in Pottery-Making Societies from Central Chile: The Contribution of Stable Isotope Analyses].
79. Y. Hamilakis, Sensorial assemblages: Affect, memory and temporality in assemblage thinking. *Camb. Archaeol. J.* **27**, 169–182 (2017).
80. J. V. Murra, Cloth and its functions in the Inca state. *Am. Anthropol.* **64**, 710–728 (1962).
81. T. L. Bray, "The commensal politics of early states and empires," in *The Archaeology and Politics of Food and Feasting in Early States and Empires*, T. L. Bray, Ed. (Springer US, 2003), pp. 1–13. https://doi.org/10.1007/978-0-306-48246-5_1.
82. K. J. Knudson, K. R. Gardella, J. Yaeger, Provisioning Inka feasts at Tiwanaku, Bolivia: The geographic origins of camelids in the Pumapunku complex. *J. Archaeol. Sci.* **39**, 479–491 (2012).
83. C. Morris, "Storage, supply, and redistribution in the economy of the Inka state," in *Anthropological History of Andean Polities*, J. V Murra, N. Wachtel, J. Revel, Eds. (Cambridge Univ. Press, 1986), pp. 59–68. https://cambridge.org/core/product/D26FF671B40E34F6A6DD3C79EC5123B0.
84. A. Ramos Gavilan, *Historia Del Célebre Santuario de Nuestra Señora de Copacabana, y Sus Milagros, e Invención de La Cruz de Carabuco (1621)* (Archivo y Biblioteca Nacionales de Bolivia–Fundación Cultural Banco Central de Bolivia, Sucre, 2015). [History of the Famous Sanctuary of Our Lady of Copacabana, Its Miracles, and the Discovery of the Cross of Carabuco (1621)].
85. G. E. Mazziotti, A. P. Vargas, Estudio médico-tanatológico de la momia del Cerro Nevado del Chuscha. *Anales de Arqueología y Etnología* **56-58**, 81–90 (2001).
86. A. S. Sanhueza, L. M. Pérez, J. J. Díaz, D. M. Busel, M. Castro, A. T. Pierola, Paleoradiología: Estudio Imagenológico del Niño del Cerro El Plomo. *Revista Chilena de Radiología* **11(4)**, 184–190 (2005). [Paleoradiology: Imaging Study of the Boy from Cerro El Plomo].
87. P. D. Horne, "The Prince of El Plomo: A frozen treasure," in *Human Mummies*, K. Spindler, H. Wilfing, E. Rastbichler-Zissernig, D. zur Nedden, H. Nothdurfter, Eds. (Springer Vienna, 1996), pp. 153–157.
88. J. L. Faux, Hail the conquering gods: Ritual sacrifice of children in Inca society. *J. Contemp. Anthropol.* **3**, 1 (2012).
89. A. S. Wilson, E. L. Brown, C. Villa, N. Lynnerup, A. Healey, M. C. Ceruti, J. Reinhard, C. H. Previgliano, F. A. Araoz, J. Gonzalez Diez, T. Taylor, Archaeological, radiological, and biological evidence offer insight into Inca child sacrifice. *Proc. Natl. Acad. Sci. U.S.A.* **110**, 13322–13327 (2013).
90. O. Kawchuk, Children of heaven : A bioarchaeological review of the Inca Capacocha mummies. *USURJ* **6**, 1–8 (2019).
91. J. W. Verano, "8. The physical evidence of human sacrifice in ancient Peru," in *Ritual Sacrifice in Ancient Peru*, E. P. Benson, A. G. Cook, Eds. (University of Texas Press, 2001), pp. 165–184.
92. V. A. Andrushko, M. R. Buzon, A. M. Gibaja, G. F. McEwan, A. Simonetti, R. A. Creaser, Investigating a child sacrifice event from the Inca heartland. *J. Archaeol. Sci.* **38**, 323–333 (2011).
93. A. Ruchonnet, M. Diehl, Y.-H. Tang, E. F. Kranioti, Cranial blunt force trauma in relation to the victim's position: An experimental study using polyurethane bone spheres. *Forensic Sci. Int.* **301**, 350–357 (2019).
94. J. de Betanzos, *Narrative of the Incas [1551]* (University of Texas Press, 1996).
95. J. Reinhard, C. Ceruti, Rescue archaeology of the Inca mummy on Mount Quehuar, Argentina. *J. Biol. Res.* **80**, 303–307 (2006).
96. P. Cieza de León, *Crónica Del Perú [1553]* (Editorial Peisa, 1988). [Chronicle of Peru].
97. M. E. Gentile Lafaille, Dimensión sociopolítica y religiosa de la capacocha del cerro Aconcagua. *Bull. Inst. Fr. Études Andines* **25**, 43–90 (1996). [The Sociopolitical and Religious Dimension of the Capacocha of Cerro Aconcagua].
98. D. M. Socha, J. Reinhard, R. C. Perea, Inca human sacrifices from the Ampato and Pichu Pichu volcanoes, Peru: New results from a bio-anthropological analysis. *Archaeol. Anthropol. Sci.* **13**, 94 (2021).
99. J. Reinhard, M. C. Ceruti, *Investigaciones Arqueológicas En El Volcán Llullaillaco: Complejo Ceremonial Incaico de Alta Montaña* (BPR Publishers, 2000). [Archaeological Investigations on Llullaillaco Volcano: The High-Mountain Inca Ceremonial Complex].
100. E. Johnstone-Belford, S. J. Fallon, J. F. Dipnall, S. Blau, The importance of bone sample selection when using radiocarbon analysis in cases of unidentified human remains. *Forensic Sci. Int.* **341**, 111480 (2022).
101. S. F. Renard, Objetos textiles, pasos y caminantes trasandinos. *Estud. Atacameños* , 291–305 (2018). [Textile Objects, Mountain Passes, and Trans-Andean Travelers].
102. H. Horta Tricallotis, La ofrenda de estatuillas en el rito de la capacocha y su relación con el mito del origen de los Incas. *Lat. Am. Antiq.* **35**, 346–366 (2024). [The Offering of Statuettes in the Capacocha Rite and Its Relationship to the Myth of the Origin of the Incas].
103. D. Bachraty, Estéticas rituales., Nuevos antecedentes acerca del uso de la ccahua o unku negro del Niño del cerro El Plomo. *Rev. Chil. Antropol.*, 269–284 (2021). [Ritual Aesthetics: New Evidence on the Use of the ccahua or Black Unku of the Boy from Cerro El Plomo].
104. S. Hoces de la Guardia Ch., A. M. Rojas Z., Vestimenta de mujeres en la nobleza Inca. Ajuar textil en el enterratorio del Cerro Esmeralda y sus relaciones con los textiles en miniatura de estatuillas. *Nuevo Mundo Mundos Nuevos, Colloques* (2016). Available at http://journals.openedition.org/nuevomundo/69833. [Women's Dress among the Inca Nobility: Textile Grave Goods in the Cerro Esmeralda Burial and Their Relationship to Miniature Textiles on Statuettes].
105. D. Bachraty, C. Nautré, La capacocha de cerro Esmeralda. Relaciones textiles, identitarias e ideológicas en torno al culto de Huantajaya. *Boletín del Museo Chileno de Arte Precolombino* **28**, 129–147 (2023). [The Capacocha of Cerro Esmeralda: Textile, Identity, and Ideological Relations Surrounding the Cult of Huantajaya].
106. A. M. Rojas, S. Hoces de la Guardia, La unidad de un conjunto simbólico. Los textiles del enterratorio incaico Cerro Esmeralda. *Boletín de la Sociedad Chilena de Arqueología* **53**, 14–40 (2022). [The Unity of a Symbolic Ensemble: The Textiles from the Inca Burial of Cerro Esmeralda].
107. V. Cereceda, ¿De transiciones y pachacutis?: Un pequeño diseño en vestimentas de figuritas de ceremonias de altura. *Boletín del Museo Chileno de Arte Precolombino* **25**, 271–314 (2020). [Of Transitions and Pachacutis? A Small Design in the Garments of Figurines from High-Altitude Ceremonies].
108. V. Cereceda Bianchi, Festones en pequeñas vestimentas de enterratorios de altura (Capacocha). *Zea Books*, 10.32873/unl.dc.zea.1623 (2024). [Festoons in Small Garments from High-Altitude Burials (Capacocha)].
109. P. Richardin, M. Coudert, N. Gandolfo, J. Vincent, Radiocarbon dating of mummified human remains: Application to a series of Coptic mummies from the Louvre Museum. *Radiocarbon* **55**, 345–352 (2013).
110. L. Cornejo, Sobre la cronología de la imposición cuzqueña en Chile. *Estud. Atacameños*, 101–116 (2014). [On the Chronology of the Cuzco Imposition in Chile].
111. A. García, C. Greco, R. A. Moralejo, P. A. Ochoa, Aplicación de estadística bayesiana al estudio de la cronología de la expansión incaica en Argentina. *Arqueología* **29**, 11140 (2023). [Application of Bayesian Statistics to the Study of the Chronology of Inca Expansion in Argentina].
112. E. J. Marsh, R. Kidd, D. Ogburn, V. Durán, Dating the expansion of the Inca Empire: Bayesian models from Ecuador and Argentina. *Radiocarbon* **59**, 117–140 (2017).
113. A. García, R. A. Moralejo, P. A. Ochoa, Radiocarbon chronology of the Inca expansion in Argentina. *Antípoda. Revista de Antropología y Arqueología* **51-83**, (2021).
114. F. Garrido, A chronological model for Inca Provincial Expansion: The case of the Copiapo Valley. *Lat. Am. Antiq.* **36**, 100–119 (2024).
115. B. Murphy, D. Salazar, M. W. Dee, F. M. Hayashida, A. Troncoso, C. Parcero-Oubiña, J. Berenguer, P. Erdil, A high-precision radiocarbon chronology of Inka rule in the Upper Loa River Region of northern Chile. *Radiocarbon* **66**, 676–698 (2024).
116. J. H. Rowe, *An Introduction to the Archaeology of Cuzco* (Peabody Museum Press, 1944); https://viewer.lib.harvard.edu/viewer/URN-3:FHCL:26542153?n=1.
117. A. Meyers, Inca archaeology and the Late Horizon: Some polemic remarks. *Tambo. Boletín de Arqueología* **255-282**, (2016).
118. R. Barberena, L. Menéndez, P. J. le Roux, E. J. Marsh, A. Tessone, P. Novellino, G. Lucero, J. Luyt, J. Sealy, M. Cardillo, A. Gasco, C. Llano, C. Frigolé, D. Guevara, G. Da Peña, D. Winocur, A. Benítez, L. Cornejo, F. Falabella, C. Méndez, A. Nuevo-Delaunay, L. Sanhueza, F. S. Sagredo, A. Troncoso, S. Zárate, V. A. Durán, V. Cortegoso, Multi-isotopic and morphometric evidence for the migration of farmers leading up to the Inka conquest of the southern Andes. *Sci. Rep.* **10**, 21171 (2020).
119. D. Bachraty, La capacocha del volcán Sara Sara: Descripción y análisis de los objetos ofrendados y del contexto ritual. *Boletín de Arqueología PUCP* , 91–107 (2025).
120. J. Reinhard, C. Ceruti, Sacred mountains, ceremonial sites and human sacrifice among the Incas. *Archeoastronomy* **19**, 1–43 (2005).
121. T. C. O'Connell, R. E. M. Hedges, M. A. Healey, A. H. R. W. Simpson, Isotopic comparison of hair, nail and bone: Modern analyses. *J. Archaeol. Sci.* **28**, 1247–1255 (2001).
122. S. N. Rodionov, A sequential algorithm for testing climate regime shifts. *Geophys. Res. Lett.* **31**, L09204 (2004).
123. E. M. Gayo, V. B. McRostie, R. Campbell, C. Flores, A. Maldonado, M. Uribe-Rodriguez, P. I. Moreno, C. M. Santoro, D. A. Christie, A. A. Muñoz, L. Gallardo, Geohistorical records of the Anthropocene in Chile. *Elementa* **7**, 15 (2019).
124. S. N. Rodionov, Use of prewhitening in climate regime shift detection. *Geophys. Res. Lett.* **33**, L12707 (2006).
125. A. Fedorov, R. Beichel, J. Kalpathy-Cramer, J. Finet, J.-C. Fillion-Robin, S. Pujol, C. Bauer, D. Jennings, F. Fennessy, M. Sonka, J. Buatti, S. Aylward, J. V. Miller, S. Pieper, R. Kikinis, 3D slicer as an image computing platform for the quantitative imaging network. *Magn. Reson. Imaging* **30**, 1323–1341 (2012).
126. T. Bhavsar, S. Prakash, 3D-printing of skull bone from CT scan data. *Mater. Today Proc.* **28**, 2447–2451 (2020).

127. S. Roth, J. S. Raul, J. Ruan, R. Willinger, Limitation of scaling methods in child head finite element modelling. *Int. J. Vehicle Saf.* **2**, 404 (2007).
128. H. Delye, T. Clijmans, M. Y. Mommaerts, J. V. Sloten, J. Goffin, Creating a normative database of age-specific 3D geometrical data, bone density, and bone thickness of the developing skull: A pilot study. *J. Neurosurg. Pediatr.* **16**, 687–702 (2015).
129. D. De Kegel, A. Meynen, N. Famaey, G. Harry van Lenthe, B. Depreitere, J. Vander Sloten, Skull fracture prediction through subject-specific finite element modelling is highly sensitive to model parameters. *J. Mech. Behav. Biomed. Mater.* **100**, 103384 (2019).
130. A. G. Hogg, T. J. Heaton, Q. Hua, J. G. Palmer, C. S. Turney, J. Southon, A. Bayliss, P. G. Blackwell, G. Boswijk, C. Bronk Ramsey, C. Pearson, F. Petchey, P. Reimer, R. Reimer, L. Wacker, SHCal20 Southern Hemisphere calibration, 0–55,000 years cal BP. *Radiocarbon* **62**, 759–778 (2020).
131. J. Haslett, A. Parnell, A simple monotone process with application to radiocarbon-dated depth chronologies. *J. R. Stat. Soc. C* **57**, 399–418 (2008).
132. M. Stuiver, P. J. Reimer, Extended 14 C data base and revised CALIB 3.0 14 C age calibration program. *Radiocarbon* **35**, 215–230 (1993).

Acknowledgments: We thank our collaborating institutions—Clínica Alemana de Santiago (Chile), the Max Planck Institute for Evolutionary Anthropology (Germany), and the University of Bradford (United Kingdom)—for support in conducting the analyses reported in this study. We also thank the Consejo de Monumentos Nacionales de Chile (Chile) for authorizing the international export of archaeological samples under Exempt Decree No. 7, which was essential for completing this research. We are grateful to P. Monteverde, M. Alarcón, and J. Gamboa for photographic contributions. We also thank Andesjournal for the image that inspired our proposed cover image, and we especially acknowledge Katiushka Loyola for creating the cover illustration. We further thank the Museo Regional de Iquique (Chile) and the Museo Nacional de Historia Natural (Chile) for supporting this investigation and facilitating access to archaeological collections. M.S. acknowledges support from UMR 8096 ArchAm, CNRS–Paris 1 (France). **Funding:** V.S.-P. acknowledges support from the FAIP-N-43-INV project of the Servicio Nacional del Patrimonio Cultural. E.M.G. acknowledges support from ANID FONDAP 1523A0002 and ANID PIA/BASAL FB210006. M.S. acknowledges support from ANID FONDECYT 1240764. D.C.S.-G. acknowledges funding from the Generalitat Valenciana (CIDEGENT/2019/061). **Author contributions:** Conceptualization: V.S.-P., M.S., E.M.G., P.M.-Q., M.C., M.L.C., X.S., and D.C.S.-G. Methodology: V.S.-P., E.M.G., P.M.-Q., M.C., G.M.R.-C., M.L.C., V.C., C.S., X.S., and D.C.S.-G. Software: E.M.G. and G.M.R.-C. Validation: V.S.-P., M.S., E.M.G., M.L.C., and D.C.S.-G. Formal analysis: V.S.-P., E.M.G., P.M.-Q., G.M.R.-C., M.L.C., A.W., V.C., C.S., X.S., and D.C.S.-G. Investigation: V.S.-P., M.S., M.C., L.P.M., M.L.C., A.W., V.C., C.S., X.S., and D.C.S.-G. Resources: V.S.-P., E.M.G., M.C., M.L.C., C.S., X.S., P.S., and D.C.S.-G. Data curation: V.S.-P., E.M.G., M.L.C., and D.C.S.-G. Writing—original draft: V.S.-P., M.S., E.M.G., M.C., L.P.M., G.M.R.-C., and M.L.C. Writing—review and editing: V.S.-P., M.S., E.M.G., P.M.-Q., M.C., L.P.M., G.M.R.-C., M.L.C., A.W., V.C., C.S., X.S., and D.C.S.-G. Visualization: V.S.-P., E.M.G., G.M.R.-C., and M.L.C. Supervision: V.S.-P. and D.C.S.-G. Project administration: V.S.-P., M.S., and D.C.S.-G. Funding acquisition: V.S.-P., M.S., E.M.G., L.P.M., and D.C.S.-G. **Competing interests:** The authors declare that they have no competing interests. **Data, code, and materials availability:** All data and code needed to evaluate and reproduce the results in the paper are present in the paper and/or the Supplementary Materials. This study did not generate new materials.

Submitted 24 June 2025
Accepted 2 June 2026
Published 15 July 2026
10.1126/sciadv.adz9055

Science Advances

Pilgrimage to sacrifice: Mechanisms, causes, and time of death of the Western Andean Capacocha of the Southern Tawantinsuyu

Verónica Silva-Pinto, Marcela Sepúlveda, Eugenia M. Gayo, Pablo Mendez-Quiros, Mario Castro, Lumila Paula Menéndez, Gonzalo M. Rojas-Costa, María L. Cerón, Andrew S. Wilson, Verónica Catalán, Claudio Silva, Ximena Stecher, Pablo Soffia, and Domingo C. Salazar-García

Sci. Adv. **12** (29), eadz9055. DOI: 10.1126/sciadv.adz9055

Science Advances (ISSN 2375-2548) is published by the American Association for the Advancement of Science. 1200 New York Avenue NW, Washington, DC 20005. The title *Science Advances* is a registered trademark of AAAS.